# Peroxy radicals during BERLIOZ at Pabstthum: Measurements, radical budgets and ozone production

D. Mihelcic, <sup>1</sup> F. Holland, <sup>1</sup> A. Hofzumahaus, <sup>1</sup> L. Hoppe, <sup>1</sup> S. Konrad, <sup>1</sup> P. Müsgen, <sup>1</sup> H.-W. Pätz, <sup>1</sup> H.-J. Schäfer, <sup>1</sup> T. Schmitz, <sup>1</sup> A. Volz-Thomas, <sup>1</sup> K. Bächmann, <sup>2</sup> S. Schlomski, <sup>2</sup> U. Platt, <sup>3</sup> A. Geyer, <sup>3</sup> B. Alicke, <sup>3</sup> and G. K. Moortgat<sup>4</sup>

Received 2 July 2001; revised 5 March 2002; accepted 2 April 2002; published 13 February 2003.

[1] The Photochemistry Experiment during BERLIOZ (PHOEBE) was conducted in July and August 1998 at a rural site located near the small village of Pabstthum, about 50 km northwest of downtown Berlin. In this paper, spectroscopic measurements of hydroxyl (OH) and peroxy radicals (HO<sub>2</sub> and RO<sub>2</sub>) are discussed for two intensive days (20 and 21 July) of the campaign. On both days peak values of the radical concentrations were similar, reaching  $6-8 \times 10^6$  cm<sup>-3</sup> for OH and 20-30 ppt for RO<sub>2</sub> and HO<sub>2</sub>. Fairly high OH concentrations were observed during the morning hours in the presence of high-NO<sub>x</sub> mixing ratios (>20ppb). The "master chemical mechanism" (MCM) was used to calculate OH, HO<sub>2</sub>, and RO<sub>2</sub> concentrations from the simultaneously measured data comprising a comprehensive set of speciated hydrocarbons and carbonyl compounds, O<sub>3</sub>, CO, NO, NO<sub>2</sub>, HONO, PAN, J(NO<sub>2</sub>), J(O<sup>1</sup>D), and meteorological parameters. The calculated OH concentrations are in excellent agreement with the measurements during the morning hours at high-NO<sub>x</sub> (>10 ppb). However, at low NO<sub>x</sub> conditions the model overestimates OH by a factor 1.6. The modeled concentrations of HO<sub>2</sub> and RO<sub>2</sub> are in reasonable agreement with the measurements on 20 July. On the next day, when isoprene from nearby sources was the dominant VOC, the model overpredicted HO2 and RO2 in addition to OH. Radical budgets solely calculated from measured data show that a missing sink for OH must be responsible for the overestimation by MCM. Missing VOC reactivity is unlikely, unless these VOC would not lead to RO<sub>2</sub> production upon reaction with OH. The measured RO<sub>2</sub>/HO<sub>2</sub> ratio of about one is well reproduced by the MCM, whereas a simple model without recycling of RO<sub>2</sub> from decomposition and isomerisation of alkoxy radicals underpredicts the measured ratio by about a factor of two. This finding highlights the importance of RO<sub>2</sub> recycling in the chemical mechanism. The ozone production rate P(O<sub>3</sub>), calculated from the peroxy radical concentrations and NO, had a maximum of 8 ppb/hr at 0.5 ppb NO, which is in good agreement with results from previous campaigns at Tenerife and Schauinsland. INDEX TERMS: 0365 Atmospheric Composition and Structure: Troposphere—composition and chemistry; 0345 Atmospheric Composition and Structure: Pollution—urban and regional (0305); 0322 Atmospheric Composition and Structure: Constituent sources and sinks; KEYWORDS: hydroxyl radical, peroxy radicals, radical budgets, ozone production, photochemistry

**Citation:** Mihelcic, D., et al., Peroxy radicals during BERLIOZ at Pabstthum: Measurements, radical budgets and ozone production, *J. Geophys. Res.*, 108(D4), 8254, doi:10.1029/2001JD001014, 2003.

#### 1. Introduction

[2] The hydroxyl radical (OH) is the major tropospheric oxidant and is responsible for the chemical degradation of

Copyright 2003 by the American Geophysical Union. 0148-0227/03/2001JD001014

many atmospheric trace gases and pollutants [Levy, 1971; Logan et al., 1981; Ehhalt et al., 1991]. Peroxy radicals (HO<sub>2</sub> and RO<sub>2</sub>, where R represents an organic group) are produced by reactions of OH with CO and volatile organic compounds (VOC) and play a central role in the photochemical formation of ozone in the troposphere [Chameides and Walker, 1973; Crutzen, 1979, Trainer et al., 1987].

[3] In recent years, measurements of OH, HO<sub>2</sub>, and the sum of HO<sub>2</sub> + RO<sub>2</sub> have become available in a number of field studies, which were designed to test our understanding of the fast photochemistry in the planetary boundary layer. The experiments were performed at different sites in clean Antarctic [Jefferson et al., 1998; Chen et al., 2001] and

<sup>&</sup>lt;sup>1</sup>Institut für Chemie und Dynamik der Geosphäre, Forschungszentrum Jülich, Jülich, Germany.

<sup>&</sup>lt;sup>2</sup>Technische Hochschule Darmstadt, Darmstadt, Germany.

<sup>&</sup>lt;sup>3</sup>Ruprecht-Karls-Universität Heidelberg, Institut für Ümweltphysik, Heidelberg, Germany.

<sup>&</sup>lt;sup>4</sup>Max-Planck-Institut für Chemie, Division of Atmospheric Chemistry, Mainz, Germany.

marine environments [e.g., Hauglustaine et al., 1999; Carslaw et al., 1999; Kanaya et al., 2000; Brauers et al., 2001], in clean continental regions [Poppe et al., 1994; McKeen et al., 1997; Ehhalt, 1999;], and in forested areas [Carslaw et al., 1999; Tan et al., 2001]. One study has been reported which was performed in polluted urban air [George et al., 1999].

- [4] In only few of the ground-based studies both OH and HO<sub>2</sub> were measured. In the Tropospheric OH Photochemistry Experiment (TOPHE) carried out in the Rocky Mountains of Colorado in 1993, OH concentrations were measured by long-path absorption and by ion-assisted mass spectrometry [Mount and Williams, 1997; Tanner et al., 1997]. HO<sub>2</sub> was measured by conversion into OH, which was subsequently detected by laser-induced fluorescence [Stevens et al., 1997], and the sum of HO<sub>2</sub> and RO<sub>2</sub> was measured by a chemical amplifier [Cantrell et al., 1997]. In this study the chemical model overpredicted the OH concentrations by 50% on average [McKeen et al., 1997], and the modeled HO<sub>2</sub> concentrations were higher than the measurements by up to a factor of 3 [Cantrell et al., 1997]. The measured ratio RO<sub>2</sub>/HO<sub>2</sub> was 3-4 times greater than expected under clean conditions, and over a factor of 10 higher than predictions under polluted conditions [Stevens et al., 1997].
- [5] In the Los Angeles Free Radical Experiment (LAFRE) OH and HO<sub>2</sub> concentrations were measured in polluted urban air by the FAGE technique in 1993 [George et al., 1999]. The observations were compared with model calculations, which used a surrogate species chemical mechanism. Early and late in the day, the model yielded good agreement with the measured OH and HO<sub>2</sub> concentrations. However, during midday the model results were too high by a factor of 1.5–2. Using the measured HO<sub>2</sub> concentrations as model input resulted in an improved agreement between modeled and measured OH.
- [6] The Eastern Atlantic Summer Experiment (EASE 96) was performed in the marine environment at the Mace Head Atmospheric Observatory in 1996. OH and HO<sub>2</sub> were measured by the FAGE (fluorescence assay by gas expansion) technique and the sum of RO<sub>2</sub> + HO<sub>2</sub> was recorded by a chemical amplifier [Carslaw et al., 1999]. The measurements were compared with the results of a model [Carslaw et al., 1999] based on the detailed Master Chemical Mechanism (MCM) by Jenkin et al. [1997]. For OH the model predictions were too high by about 40%. For HO<sub>2</sub> the predictions were in good agreement with the measurements on one day, but were greater than the observations by as much as a factor of 6 on another day. For RO<sub>2</sub> + HO<sub>2</sub> a general good agreement was found between the measured and modeled concentrations over a wide range of conditions.
- [7] In the Photochemistry, Emissions, and Transport (PROPHET) experiment OH and HO<sub>2</sub> were measured by the laser-induced fluorescence technique in northern Michigan in 1998 [*Tan et al.*, 2001]. The measurement site was located in a deciduous forest marked by relatively low NO<sub>x</sub> levels and high isoprene emissions [*Carroll et al.*, 2001]. The measured OH and HO<sub>2</sub> concentrations were compared to the results of a model [*Tan et al.*, 2001], which was derived from the Regional Acid Deposition Mechanism (RADM) [*Stockwell et al.*, 1997] and modified to include

the oxidation of isoprene and other biogenic VOC. Unlike in the TOHPE, LAFRE, and EASE96 campaigns, the modeled OH concentrations were generally smaller, rather than higher, when compared to the observed OH. On average the model under prediction was a factor 2.7. For HO<sub>2</sub> the model results were in good agreement with the measurements. Thus modeled HO<sub>2</sub>/OH ratios were 2.5–4 times higher than observed.

[8] In the present paper we report measurements and model calculations of OH, HO2, and RO2 from a local photochemistry study (PHOEBE), which was performed in the Berlin Ozone experiment (BERLIOZ) in summer 1998. BERLIOZ was a major activity in the area around the city of Berlin (Germany) and aimed to study the transport and chemical processes which control the formation of ozone and photooxidants in the city plume. At Pabstthum, which was one of several measurement sites in the Berlin area, comprehensive in situ measurements of radicals (OH, HO<sub>2</sub>, RO<sub>2</sub>, and NO<sub>3</sub>) were performed, in order to study their fast chemistry in a rural environment under the influence of urban pollution [Volz-Thomas et al., 2003a]. It is the first field experiment where all radicals were measured by at least one direct spectroscopic technique. Along with the radical data, a comprehensive set of measurements of NO, NO<sub>2</sub>, NO<sub>v</sub>, HONO, PAN, O<sub>3</sub>, H<sub>2</sub>O, H<sub>2</sub>O<sub>2</sub>, ROOH, CO, VOC, SO<sub>2</sub>, and photolysis frequencies among them J(O¹D)  $(O_3 \rightarrow O(^1D))$  and  $J(NO_2)$   $(NO_2 \rightarrow NO)$  were obtained. The speciated VOC measurements include alkanes, alkenes, isoprene, α-pinene, ethyne, aromatics, formaldehyde, other carbonyl compounds, and carboxylic acids. In the following we focus our analysis on the daytime chemistry of OH, HO<sub>2</sub>, and RO<sub>2</sub>, whereas the nighttime chemistry, including reactions of NO<sub>3</sub>, is presented in a companion paper by Geyer et al. [2003]. The daytime radical concentrations and their ratios are compared for two days (20 and 21 July) with model results, using an updated master chemical mechanism (MCM). The two days were characterized by high-NO<sub>x</sub> (up to 30 ppb) in the morning and high isoprene levels (several hundred ppt) on the second day. Unlike in previous studies, speciated radical data from the measurements are used to investigate the radical budgets and the ozone production rate. The ozone formation is compared with field data obtained earlier at other sites (Tenerife, Schauinsland) in Europe.

#### 2. Experimental Methods

[9] The PHOEBE measurement site was located in a rural area near the small village Pabstthum ( $52.9^{\circ}$ N,  $12.9^{\circ}$ E) at about 50 km in the North-West of the city center of Berlin. The station was set up on the western border of a flat grassland ( $7.5 \times 4.5 \text{ km}^2$ ). A mixed forest dominated by Scots pine extended from the station in westerly and northerly direction. A description of the location, the arrangement of the instruments and details of the measurements can be found in the overview paper [*Volz-Thomas et al.*, 2003a] and in the other papers of this special section.

#### 2.1. Peroxy Radical Measurements

[10] The peroxy radicals were measured by Matrix Isolation and Electron Spin Resonance Spectroscopy (MIESR). The method is described in detail by *Mihelcic et al.* [1985,

Table 1. Chemical Species and Photolysis Frequencies Used as Model Input Parameters or for the Radical Budget Calculations<sup>a</sup>

Parameter	Instrument	Time Resolution	Institution	Reference
	Odd Nitrogen Compounds			
NO	chemiluminescence (770 Alppt, EcoPhysics)	1 min	FZJ	A
$NO_2$	CLD 770 Alppt + PLC 760 (EcoPhysics)	1 min	FZJ	A
$HNO_2$	DOAS 1	30 min	IUP	F
PAN	GC-ECD (Meteorologieconsult)	6 min	FZJ	A
	Other			
$O_3$	UV-Absorption (TE-49)	1 min	FZJ	A
CO	IR-Absorption (TE-48)	1 min	FZJ	A
$H_2$	not measured; 500 ppb			
Aerosol	Pallas Optical Counter (PCS 2000)	5 min	IUP	G
	Organic Compounds			
CH <sub>4</sub>	not measured; 1.8 ppm			
NMHC: C <sub>5</sub> -C <sub>10</sub>	In situ-GC (Airmotec HC1010)	20 min	FZJ	В
NMHC: $C_2-C_{10}$	in situ-GC (HPGC/Cryogenic sampling)	85 min	FZJ	В
H <sub>2</sub> CO	fluorescence (AeroLaser, AL4001)	1 min	FZJ	A
Carbonyl compounds	derivatisation, GC/ECD	1 h	TUD	E
Carboxylic acids	capillary electrophoresis-LIF	1 h	TUD	Е
	Free Radicals			
OH	LIF	90 s	FZJ	D
$HO_2$	LIF	90 s	FZJ	D
$HO_2$	MIESR	30 min	FZJ	C
$RO_2$	MIESR	30 min	FZJ	C
	Meteorology and Radiation			
T, rH, P, wind vector	psychrometer, wind vane, cup anemometer (Thiess)	1 min	FZJ	A
$J(O^1D), J(NO_2)$	$2\pi$ sr Filter radiometers	10 s	FZJ	D

<sup>a</sup>References are as follows: A, *Volz-Thomas et al.* [2003a]; B, *Konrad et al.* [2003]; C, this paper; D, *Holland et al.* [2003]; E, *Grossmann et al.* [2003]; F, *Alicke et al.* [2003]; G, Alicke (personal communication, 1999). FZJ, Institut für Chemie und Dynamik der Geosphäre, Forschungszentrum Jülich; IUP, Institut für Umweltphysik, Universität Heidelberg; MPI, Max Planck Institut für Chemie, Mainz; TUD, Institut für Chemie, Technische.

1990]. Briefly: During the sampling interval of 30 min, ambient air (total volume: 8 l STP) is expanded at a flow rate of 270 ml/min (STP) through a nozzle into a vacuum chamber. The radicals are trapped from the gas jet in a polycrystalline D<sub>2</sub>O matrix which is formed in situ on a cold finger at a temperature of 77 K. Speciation and quantification of the radicals is achieved in the laboratory on a Bruker ESP 300E ESR-spectrometer equipped with an ER 4109 WZS wide bore cavity. The samples are kept under vacuum at 77K during storage and during the measurement. The ESR-spectra are analyzed by a nonlinear fitting procedure [Mihelcic et al., 1990]. The MIESR method allows the speciation of HO<sub>2</sub>, CH<sub>3</sub>C(O)O<sub>2</sub> and the sum of organic peroxy radicals. The latter is denoted RO<sub>2</sub> in the following. The MIESR also provides measurements of NO<sub>2</sub> and NO<sub>3</sub>.

- [11] Over the range of concentrations encountered during BERLIOZ, the precision for  $NO_2$ ,  $NO_3$ ,  $HO_2$ ,  $CH_3C(O)O_2$ , was always better than 2 ppt. The precision for  $NO_3$  radicals was better than 1 ppt, because of its narrower line width. The systematic uncertainty of the MIESR measurements was estimated from absolute calibrations made in the laboratory to be  $\pm 5\%$  [Mihelcic et al., 1985, 1990; Geyer et al., 1999, 2003].
- [12] The MIESR sampler was mounted on a pneumatic mast, using a ball bearing and a wind-vane to ensure that the inlet nozzle pointed into the wind in order to avoid contamination or losses of the radicals on the surface of the sampler. The inlet of the sampler was 11.5 m above the surface during sampling. Due to the limited number of samples that could be stored for later analysis, measurements by MIESR were concentrated on the intensive

observational periods which took place on 20–21 July and in the night from 4 to 5 July 1998.

#### 2.2. Other Radical Measurements

[13] The total peroxy radical concentration  $(HO_2 + RO_2)$  was also measured at Pabstthum by a Chemical Amplifier (CA) deployed by the Max-Planck Institute for Chemistry, Mainz [Volz-Thomas et al., 2003b]. The concentrations of OH and  $HO_2$  radicals were measured by Laser Induced Fluorescence (LIF) [Holland et al., 2003]. The LIF instrument sampled ambient air by gas expansion through a nozzle at about 10 m above ground. OH was measured directly by resonance fluorescence following excitation at 308 nm.  $HO_2$  was first converted chemically into OH, which was subsequently detected by LIF. The time resolution of the measurements was 1.5 min and the estimated calibration error  $\pm 20\%$   $(2\sigma)$ .

# 2.3. Other Trace Gases and Parameters

[14] A comprehensive set of trace gases, photolysis frequencies, and meteorological parameters was measured during PHOEBE [cf., *Volz-Thomas et al.*, 2003a] (Table 1). The parameters used in this paper for model initialization and radical budget calculations are listed in Table 1 together with the appropriate references. NO and NO<sub>2</sub> were measured by chemiluminescence and a photolytic converter (accuracy 5% and 5% for NO and NO<sub>2</sub>, respectively). O<sub>3</sub> and CO concentrations were measured using two identical standard UV-photometers (TE-49) and a slightly modified infrared filter correlation instrument (TE-48), respectively. Peroxyacetylnitrate (PAN) was measured by gas chroma-

tography with an electron capture detector (accuracy < 10%). Nitrous acid (HONO) was measured using Differential Optical Absorption Spectroscopy (DOAS; limit of detection: 80 ppt; accuracy  $\pm 6\%$ ,  $1\sigma$ ). More than 60 hydrocarbons (HC) in the range of C<sub>2</sub>-C<sub>10</sub> were measured by using two in situ GC systems [Konrad et al., 2003]. The measurements included alkanes, alkenes, isoprene,  $\alpha$ pinene, ethyne, and aromatic compounds. Combining the data sets from the two instruments NMHC records with a time resolution of 20 min were obtained. Carbonyl compounds (C<sub>2</sub> to C<sub>10</sub>) were measured by a novel sampling technique, followed by analysis via gas chromatography. The data sets provide information on a large number of aliphatic and olefinic alkanals, including hydroxycarbonyls and dicarbonyls, benzaldehyde and pinonaldehyde [Grossmann et al., 2003]. Formaldehyde was measured using a fluorescence instrument (AeroLaser) based on the Hantzsch reaction and by the DOAS instrument. Photolysis Frequencies of  $O_3 \rightarrow O(^1D)$ ,  $J(O^1D)$ , and  $NO_2 \rightarrow NO$ ,  $J(NO_2)$ , were measured by  $2\pi$  sr filter radiometers and an actinic flux spectral radiometer with good agreement between the instruments [Holland et al., 2003]. Due to data gaps caused by occasional malfunctioning of the spectral radiometer, J(O<sup>1</sup>D) and J(NO<sub>2</sub>) data are taken from the filter radiometers. The estimated errors are  $\pm 14\%$  and  $\pm 9\%$ , respectively. Wind, temperature, pressure and relative humidity (rH) were measured by standard meteorological devices.

[15] All in situ measurements were made at approximately the same height as the MIESR, about 10–11 m above ground and within a horizontal distance of 20 m. The DOAS instrument employed a folded light path of 15 m base length [Alicke et al., 2003]. It was mounted in an open crane cantilever on an 8 m high platform, next to the LIF instrument container (see Figure 3 of Volz-Thomas et al. [2003a] for details).

[16] We like to note that several parameters (e.g., HO<sub>2</sub>, NO<sub>2</sub>, O<sub>3</sub>, H<sub>2</sub>CO, J(NO<sub>2</sub>)) were measured by more than one technique. In all cases good agreement was observed between the different instruments [Volz-Thomas et al., 2003a], except for formaldehyde where an unresolved discrepancy between Hantzsch and DOAS was observed with the DOAS data being systematically larger by up to a factor of two (1.3 on average) [Grossmann et al., 2003]. In the following, the data of the instruments providing the highest time resolution and located closest to the radical measurements are used, i.e. the Hantzsch data for HCHO.

# 3. Modeling Approach

# 3.1. Master Chemical Mechanism

[17] The "master chemical mechanism" (MCM) [Jenkin et al., 1997] was used to calculate the OH,  $\mathrm{HO}_2$ , and  $\mathrm{RO}_2$  radical concentrations from the photolysis frequencies and trace gases that were measured simultaneously at Pabstthum. The MCM consists of 10.500 chemical reactions involving 17 inorganic and 120 organic species. The chemical mechanism was updated in the following way: the  $\alpha$ -pinene oxidation scheme was adopted from the MCM2 model (the MCM2 model is available at http://www.chem.-leeds.ac.uk/Atmospheric/MCM). The rate coefficients for the reaction of  $\mathrm{NO}_2$  with OH, and for the reaction of  $\mathrm{O}_3$  with NO were updated according to Sander et al. [2000] and

the rate coefficient for the reaction of  $\rm HO_2$  with NO was revised to  $9.7 \times 10^{-12}~\rm cm^3~s^{-1}$  based on the measurements made by *Bohn and Zetzsch* [1997]. The photolysis frequencies which are calculated within MCM from the solar zenith angle were tied to the measurements in the following way: For  $\rm J(NO_2)$  and  $\rm J(O^1D)$ , the values measured by the two filter radiometers were used directly. The other photolysis rates were calculated in the MCM model for clear-sky conditions and then scaled with the ratio of the measured to calculated values of  $\rm J(NO_2)$ .

[18] The differential equations were integrated with the software package FACSIMILE [Curtis and Sweetenham, 1987]. The model was initialized every 5 min with the measured concentrations of NO, NO<sub>2</sub>, O<sub>3</sub>, CO, PAN, HCHO and higher carbonyl compounds, NMHCs, H<sub>2</sub>O, and aerosols, as well as temperature and photolysis frequencies (see Table 1). The initial radical concentrations were taken from the output of the previous 5 min time interval. The time depended concentrations yielded radical concentrations very close to steady state conditions.

# 3.2. Simple Quasi-Stationary State Model

[19] It is interesting to compare the radical ratios HO<sub>2</sub>/OH and RO<sub>2</sub>/HO<sub>2</sub> obtained from the MCM with calculations using a simple steady state approach based on the reactions shown in Table 2. We estimate the concentrations of the short-lived radicals species by assuming that the HO<sub>2</sub>/OH ratio is determined predominantly by radical recycling reactions. The validity of this assumption is demonstrated in section 5.1 where radical budgets are discussed. In the approximation for RO2/HO2 ratio we neglect the secondary production of peroxy radicals due to RO decomposition and isomerisation, as well as the production of RO2 and HO2 from ozonolysis, and the loss reactions due to RO2 self reactions, due to its minor contributions. Adding up the major production and loss terms for both, HO<sub>2</sub> and RO<sub>2</sub> radicals, one obtains for the steady state of HO<sub>2</sub>(14) and  $RO_2(15)$ :

$$\begin{split} -d[\text{HO}_2]/dt &= 0 = k_3[\text{OH}][\text{CO}] + k_4[\text{OH}][\text{HCHO}] \\ &+ k_{5i}[\text{RO}_2][\text{NO}] + 2J(\text{HCHO})_{\text{radical}}[\text{HCHO}] - k_2[\text{HO}_2][\text{NO}] \\ &- k_{10}[\text{RO}_2][\text{HO}_2] - k_9[\text{HO}_2][\text{HO}_2] \end{split} \tag{14}$$
 
$$-d[\text{RO}_2]/dt = 0 = k_{6i}[\text{OH}][\text{VOCi}] \\ &+ k_{12}[\text{PAN}]\{(k_{11}[\text{NO}_2]/k_{13}[\text{NO}] + 1)\}^{-1} + k_7[\text{OH}][\text{CH}_4] \\ &- k_{5i}[\text{RO}_2][\text{NO}] - k_{10}[\text{RO}_2][\text{HO}_2] \tag{15}$$

By assuming quasi steady state between  $[HO_2]$  and  $[RO_2]$ , the  $HO_2/OH$  ratio can be approximated from reactions (14) and (15):

$$\begin{split} &\frac{[HO_2]}{[OH]} \\ &\approx \frac{(k_{6i}[VOC_i] + k_3[CO] + k_4[HCHO] + k_7[CH_4] + (Q + P)/[OH])}{k_2[NO]} \end{split}$$
 (16)

The term  $P = k_{12} [PAN] \{ (k_{11}[NO_2]/k_{13}[NO]) + 1 \}^{-1}$  denotes the production of  $CH_3O_2$  from PAN decomposition

**Table 2.** List of Chemical Reactions That Have a Major Influence on the Radical Budget of OH, HO<sub>2</sub>, and RO<sub>2</sub>

Species	Radical Formation	k or J Parameter	Reaction Number
ОН	$H_2O + O(^1D) \rightarrow OH + OH$	$\mathbf{k}_1$	(1)
OH	$HONO + h\nu \rightarrow OH + NO$	$J_{(HONO)}$	. ,
OH	$HO_2 + NO \rightarrow OH + NO_2$	k <sub>2</sub>	(2)
$HO_2$	$HCHO + h\nu + O_2 \rightarrow 2HO_2 + CO$	$J_{(HCHO)}$	` '
$10_2$	$OH + CO + O_2 \rightarrow HO_2 + CO_2$	k <sub>3</sub>	(3)
$10_2$	$OH + HCHO + O_2 \rightarrow HO_2 + CO + H_2O$	$k_4$	(4)
$HO_2$	$HO_2 + NO + O_2 \rightarrow HO_2 + NO_2 + Carbonyle$	k <sub>5</sub>	(5)
$RO_2$	$OH + VOC + O_2 \rightarrow RO_2 + H_2O$	$k_6$	(6)
$RO_2$	$OH + CH_4 + O_2 \rightarrow CH_3O_2 + H_2O$	$k_7$	(7)
Species	Radical Destruction	k or J Parameter	
ЭH	$OH + NO_2 (+M) \rightarrow HNO_3 (+M)$	$k_8$	(8)
OH	$OH + VOC + O_2 \rightarrow RO_2 + H_2O$	$k_6$	(6)
OΗ	$OH + CO + O_2 \rightarrow HO_2 + CO_2$	$k_3$	(3)
OΗ	$OH + CH_4 + O_2 \rightarrow CH_3O_2 + H_2O$	k <sub>7</sub>	(7)
OΗ	$OH + HCHO + O_2 \rightarrow HO_2 + CO + H_2O$	$k_4$	(4)
$IO_2$	$HO_2 + NO \rightarrow OH + NO_2$	$k_2$	(2)
$IO_2$	$HO_2 + HO_2 \rightarrow H_2O_2 + O_2$	k <sub>9</sub>	(9)
$IO_2$	$HO_2 + RO_2 \rightarrow ROOH + O_2$	$k_{10}$	(10)
$RO_2$	$RO_2 + NO + O_2 \rightarrow HO_2 + Carbonyle + NO_2$	$k_5$	(5)
$RO_2$	$RO_2 + NO \rightarrow \alpha RONO_2$	$k_{5a}$	(5a)
$RO_2$	$RO_2 + HO_2 \rightarrow ROOH + O_2$	k <sub>10</sub>	(10)
	PAN Decomposition as Radica	! Source	
$RO_2$	$CH_3C(O)O_2 + NO_2 \rightarrow PAN$	$\mathbf{k}_{11}$	(11)
$RO_2^2$	$PAN \rightarrow CH_3C(O)O_2 + NO_2$	k <sub>12</sub>	(12)
$RO_2^{\overline{2}}$	$CH_3C(O)O_2 + NO + O_2 \rightarrow CH_3O_2 + CO_2 + NO_2$	k <sub>13</sub>	(13)

according to the reactions (11)–(13) (see Table 2). While the total PAN decomposition proceeds at a much larger rate, most of the peroxyacetyl radicals react with NO<sub>2</sub> back to PAN. The term Q denotes the HO<sub>2</sub> production from the radical channel of HCHO photolysis: Q = 2J(HCHO)<sub>radical</sub> × [HCHO]. Photolysis of the higher carbonyl compounds is neglected in (16) as it contributes less than 10% of HCHO to the peroxy radical production at Pabstthum [cf., Grossmann et al., 2003]. The OH concentration on the right side of reaction (16) is taken from the measurements. The term (Q + P)/[OH] makes a relatively small contribution and is in the range of 10 to 20% of the nominator in reaction (16).

[20] The ratio of RO<sub>2</sub> and HO<sub>2</sub> radicals is then given by reaction (17):

$$\frac{[\text{RO}_{2i}]}{[\text{HO}_{2}]} \approx \frac{\left(\frac{\underline{k}_{2}}{k_{5}}\right)}{\left\{\frac{k_{3}[\text{CO}] + 2J(\text{HCHO})_{\text{radical}}[\text{HCHO}]/[\text{OH}] + k_{4}[\text{HCHO}]}{(k_{6i}[\text{VOC}i] + P/[\text{OH}])} + 1\right\}}$$
(17)

In this simplified approach, the RO<sub>2</sub>/HO<sub>2</sub> ratio depends on the ratio of the rate constants  $k_2$  and  $k_5$  and on the ratio of the production rates for HO2 and RO2 radicals which are calculated from the measurements. The average rate coefficient for the reaction of organic peroxy radicals with NO  $k_5 \approx 8.6 \times 10^{-12} \text{ cm}^3 \text{ s}^{-1}$  is estimated from the partitioning of the organic peroxy radicals calculated by the MCM (see Figure 3).

[21] Reaction (17) provides a lower limit of the RO<sub>2</sub>/HO<sub>2</sub> ratio, because of the neglecting of the secondary production of RO<sub>2</sub> radicals from the decomposition and isomerisation of the RO intermediates. The major pathway for RO radicals in the atmosphere is the reaction with O<sub>2</sub>, forming HO<sub>2</sub> and a carbonyl compound [Atkinson, 1997] (18a). There is substantial evidence from laboratory experiments, that some of the larger RO radicals decompose through a C-C (or C-H) bond splitting (18b) or isomerise via an internal H-shift ((18c) and (18d)) at a rate that is larger than their reaction with O<sub>2</sub> [Atkinson, 1997; Le Bras, 1997]. In the presence of O<sub>2</sub>, both processes lead to new peroxy radicals, which again convert NO to NO<sub>2</sub>. As a consequence, these reactions increase the ozone formation potential of certain VOCs with respect to the primary OH attack.

$$RO + O_2 \rightarrow carbonyl + HO_2$$
 (18a)

$$RO \rightarrow R' + carbonyl$$
 (18b)

$$RO \rightarrow R*OH$$
 (18c)

$$R*OH + O_2 \rightarrow OH - R*O_2 \tag{18d}$$

Inclusion of the additional RO<sub>2</sub> production by equations (18b)-(18d) would lead to an increase in the steady state concentration of RO<sub>2</sub> and hence of the RO<sub>2</sub>/HO<sub>2</sub> ratio. However, the effect is difficult to treat quantitatively, because the effective branching ratios for reactions (18) are not well known. Vice versa, experimental quantification of the RO<sub>2</sub>/HO<sub>2</sub> ratio can help to investigate, how many organic peroxy radicals are formed upon the OH-initiated hydrocarbon oxidation.

# Results

# 4.1. Diurnal Variation of the Radical Concentrations

[22] The peroxy radical concentrations measured by MIESR during the first two intensive days of the BERLIOZ campaign (20-21 July 1998) are shown in Figure 1. Panel

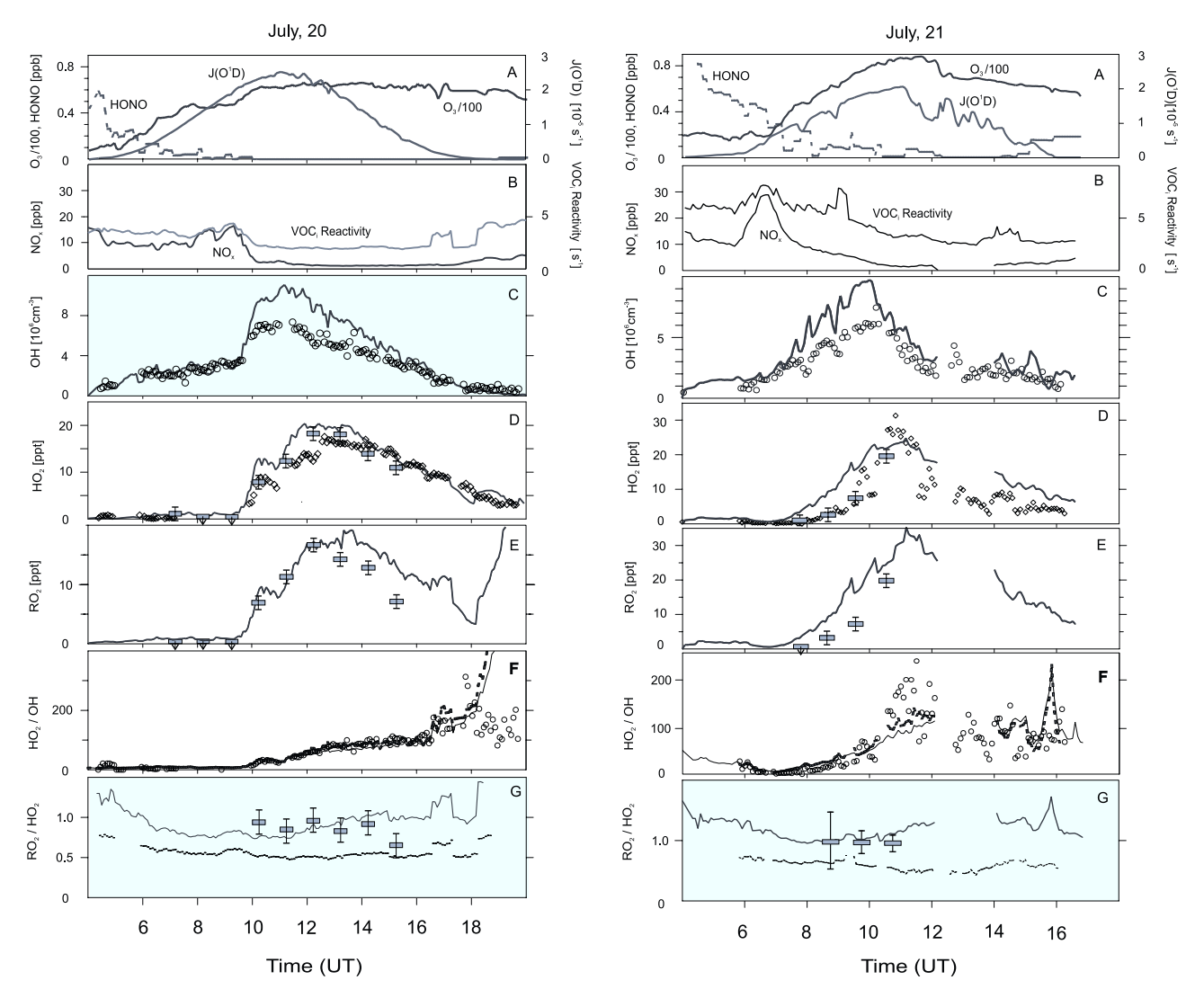


**Figure 1.** Diurnal variation of the radical concentrations and some additional parameters at Pabstthum on (left) 20 July and (right) 21 July. Panels show the following: A, HONO, O<sub>3</sub>, and J(O¹D); B, NO<sub>x</sub> and total VOC reactivity; C, OH concentration measured by LIF (open circles); D, HO<sub>2</sub> measured by LIF (open circles) and by MIESR (rectangles); E, Sum of all organic peroxy radicals (RO<sub>2</sub>) measured by MIESR (rectangles); F, HO<sub>2</sub>/OH ratio derived from the LIF data; G, RO<sub>2</sub>/HO<sub>2</sub> ratio derived from the MIESR data. The MCM results are shown as solid lines in panels C–G. The dotted lines in panels F and G are results of the simplified steady state model (equations 16 and 17).

D gives the concentration of  $HO_2$  and panel E the total concentration of organic peroxy radicals  $RO_2$ . Also shown are the OH and  $HO_2$  concentrations measured by LIF [Holland et al., 2003] in panels C and D, respectively. The upper two panels display some of the measured parameters that are important for the radical budgets, i.e.  $J(O^1D)$  [Holland et al., 2003],  $O_3$  and  $NO_x$ , [Volz-Thomas et al., 2003b], HONO [Alicke et al., 2003], and the total reactivity of the VOC toward OH, i.e.  $\Sigma([VOC_i] \cdot k_i)$  [Konrad et al., 2003]. The lowest panels show the  $HO_2/OH$  and  $RO_2/HO_2$  ratios.

[23] The first day was characterized by two different air masses with quite different chemical composition. The transition between the two regimes occurred within 30 min between 9:30 and 10:00 UT as can be seen from the  $NO_x$  mixing ratio and VOC reactivity in panel B. The

relatively high-NO<sub>x</sub> concentrations ( $\sim$ 10 ppb) at night are most likely due to local emissions from the surrounding grass lands under a shallow inversion and at low wind speeds [Glaser et al., 2003; Volz-Thomas et al., 2003b]. After break up of the inversion, the city plume of Berlin was encountered at Pabstthum around 9 UT with NO<sub>x</sub> mixing ratios of up to 18 ppb. After the air mass change, NO<sub>x</sub> dropped to levels below 5 ppb. We shall denote the two regimes as high-NO<sub>x</sub> (>10 ppb) and low-NO<sub>x</sub> (<10 ppb) in the following.

[24] The peroxy radical concentrations show qualitatively the expected anticorrelation with  $NO_x$ . At high- $NO_x$  very low concentrations at or below the detection limit (2ppt) of MIESR are found. After the air mass change, both,  $HO_2$  and  $RO_2$  start to rise and reach mixing ratios of 15–20 ppt around local noon, from where they steadily decrease in the

course of the afternoon. The HO<sub>2</sub> mixing ratio measured by LIF is in very good agreement with the MIESR data, except for the sample collected around 12:00 UT on 20 July. As discussed by [Volz-Thomas et al., 2003b], good agreement is also found for the sum of HO2 and RO2 by MIESR with the measurements made by chemical amplification. The OH concentration measured by the LIF instrument peaks about 2 hours earlier than the peroxy radicals. It is noteworthy, that OH is present at fairly large concentrations of  $(2-4) \times$  $10^6 \text{ cm}^{-3}$  during the morning hours when the NO<sub>x</sub> mixing ratio is still greater than 10 ppb. The concentration of CH<sub>3</sub>C(O)O<sub>2</sub>, which can be discriminated from the other peroxy radicals by its spectroscopic signature [Mihelcic et al., 1990], never exceeded the detection limit (2 ppt) of the MIESR. The meteorological situation on 21 July was similar to the day before, until a frontal system with scattered thunderstorms approached the region in the afternoon. In order to prevent damage by lightning strokes, the MIESR measurements were stopped at 11 UT and also the NO<sub>x</sub> measurements were switched off for calibrations between 12:20-14:00 (UT). The NO<sub>x</sub> mixing ratios in the morning were even higher than on 20 July with maximum values of about 30 ppb. The balloon soundings [Glaser et al., 2003] showed that the vertical extension of the high-NO<sub>x</sub> regime was only about 100 m. The strong decrease of NO<sub>x</sub> and other anthropogenic pollutants after 7:00 (UT) is mostly explained by the growing height of the mixed layer. The low wind speeds at ground and the wind direction preclude the explanation that the NO<sub>x</sub> was advected from Berlin as on the day before [Glaser et al., 2003]. HONO exhibited a quite similar behavior as on the previous day with a maximum in the early morning hours and a strong decay after sunrise due to increasing photolysis. Other than on 20 July, isoprene as an indicator for biogenic emissions from the nearby forest predominated the VOC's reactivity on 21 July.

[25] The diurnal variation of the radical concentrations was quite similar to that on the previous day with  $HO_2$  and  $RO_2$  peaking around local noon and OH somewhat earlier. The maximum concentrations of the peroxy radicals were somewhat larger, whereas the OH concentration was slightly lower than on 20 July. Again, relatively high-OH concentrations were observed during the morning in the presence of large  $NO_x$  mixing ratios. The faster decay of all radicals in the afternoon is consistent with the reduced UV radiation flux due to the appearance of clouds when the frontal system approached the measurement site.

# 4.2. MCM-Model Calculations of Radical Concentrations

[26] The MCM simulations of OH, HO<sub>2</sub> and RO<sub>2</sub> are compared with the measurements in Figure 1. On 20 July, the modeled OH concentrations agree with the measured data within the range of the measurement uncertainty during the time of the plume period between 6:00 and 9:30 (UT). During the transition to less polluted air, the model and the observations both show a sharp rise of OH. After the air mass has changed, the model significantly overpredicts OH by a factor 1.6 until about 16:00 (UT). For HO<sub>2</sub> the model behaves similarly with respect to the observations. During the high-NO<sub>x</sub> conditions in the morning, it agrees well with the measurements which are at the detection limit. After the

air mass has changed, the model overpredicts the measurements until about 14:30 (UT). Relative to the MIESR data the overprediction is 50% at 10:15 UT and about 10% at 11:00–13:00 UT. With respect to the LIF measurements, the overprediction is 50% around 12:00 UT. The modeled values of RO<sub>2</sub> agree with the measured data in the morning until 12:00 UT. In the afternoon there is an increasing overprediction by the model reaching a factor 1.7 at 15:00 (UT). The sharp increase in the modeled RO<sub>2</sub> concentration after 18.00 is due to the onset of nighttime chemistry when the production of RO<sub>2</sub> occurs mainly via ozonolysis and NO<sub>3</sub> reactions, as is discussed in detail by [Geyer et al., 2003].

[27] On the next day the model behaves quite similar as on the day before. While good agreement is again observed during early morning in the high-NO<sub>x</sub> regime, the model overpredicts the OH, HO<sub>2</sub>, and RO<sub>2</sub> concentrations by about a factor of two during the rest of the day. An exception is the temporary agreement of the modeled HO<sub>2</sub> data with the measurements at 11:00 UT. No comparison can be made for RO<sub>2</sub> before 7:45 UT and during the afternoon when corresponding measurements were missing.

[28] The ratio  $RO_2/HO_2$  derived from the MIESR measurements shows little variability on both days and lies mostly in the range between 0.75 and 1.0. Note that the ratio is only shown for data above the detection limit of MIESR, i.e., between 10:00–15:00 UT on 20 July and 9:00–11:00 UT on 21 July. The experimental ratios are reasonably well reproduced by the model (Figure 1), which is a consequence of the fact that the overpredictions for  $HO_2$  and  $RO_2$  cancel to a large extent. In the early morning and late evening the modeled  $RO_2/HO_2$  ratio is higher than during midday and increases to values around 1.3.

[29] The ratio HO<sub>2</sub>/OH derived from the LIF measurements on 20 July increases from about 30 in the morning to about 170 at 17:00, with decreasing NO concentrations. The ratio was typically between 10 and 60 under polluted conditions, where NO was in the range of 0.2 to 0.7 ppb, and between 80 and 140 when NO was low (0.1 to 0.2ppb). For 21 July the observed values of the HO<sub>2</sub>/OH ratio are much more scattered than on 20 July and reach maximum values of 240 around noon. The ratios observed on 20 July are reproduced within 20% by the model over the whole day until sunset. On 21 July, however, the model results resemble the observations only roughly. The model does not capture the observed variability of HO<sub>2</sub>/OH, leading to sporadic positive or negative deviations that exceed a factor of 2. The comparison of modeled and measured radical concentrations is investigated more quantitatively in Figure 2 in form of scatterplots, in which the data are filtered for high-NO<sub>x</sub> (>10ppb) and low NO<sub>x</sub> (<10ppb) conditions. In case of the peroxy radicals the high-NO<sub>x</sub> data are omitted, because the measurements were at the detection limit of the instruments, thus yielding no meaningful correlation with the model. For OH the correlations show a very similar picture on both days. At high-NO<sub>x</sub> (upper panels) there is agreement for OH within the experimental uncertainties. We like to note that HONO photolysis plays an important role during this part of the day and that neglecting this OH source would lead to a strong under prediction of OH [cf., Alicke et al., 2003]. In the low NO<sub>x</sub> regime (<10ppb), the model overpredicts OH by 50 percent or more on both days, with slightly more scatter on

21 July. For the peroxy radicals the picture at low  $NO_x$  is quite different for the two days. A relatively tight linear correlation between modeled and measured HO2 and RO2 concentrations with a slope of 1.1-1.2 is observed on 20 July. At lower HO<sub>2</sub> concentrations on 21 July the model overestimated the measurements below 10 ppt and leveled off at higher concentration. Similar behavior is suggested for the RO<sub>2</sub> concentrations. Figure 3 shows the partitioning of the organic peroxy radicals as predicted by MCM for the two days. According to the model, methylperoxy and other aliphatic RO<sub>2</sub> radicals comprise more than 50% of RO<sub>2</sub>. Oxidation of olefins and carbonyl compounds accounts for the remaining fraction. Interestingly, the peroxyacetyl mixing ratio predicted by MCM does not exceed the detection limit of the MIESR (2 ppt), which is in agreement with the measurements. Peroxy radicals from a-pinene oxidation are negligible (<1ppt) on both days. The major difference between the two days is in the fraction of RO<sub>2</sub> originating from isoprene oxidation which are unimportant on 20 July except for the late afternoon. On 21 July, isoprene oxidation accounts for 20-50% of the RO2 in the MCM over the entire day. This is due to the 5 times larger isoprene mixing

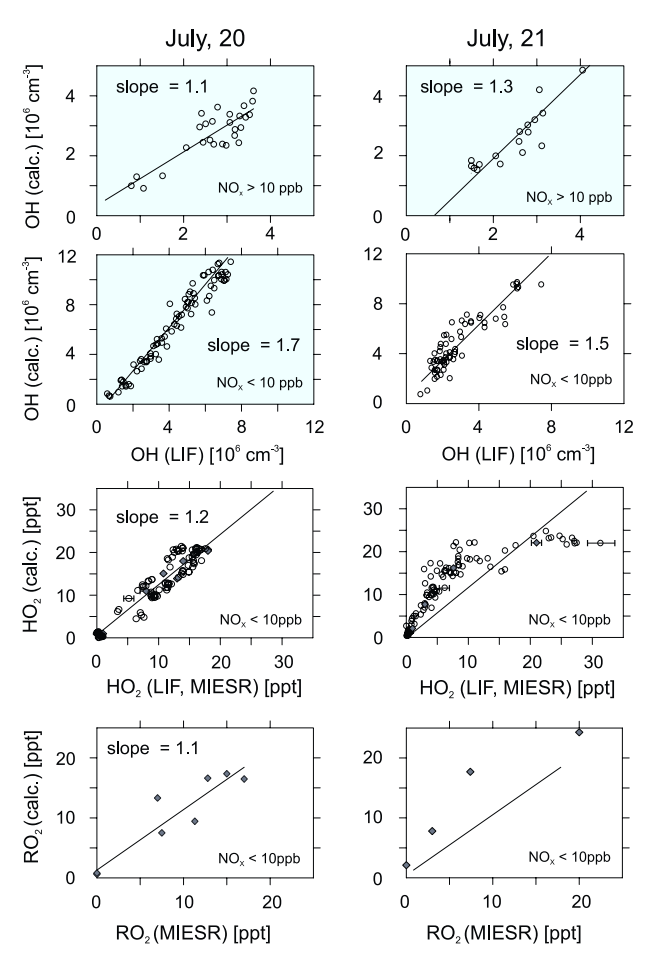


**Figure 2.** Correlation of calculated (MCM) and measured radical concentrations at Pabstthum for (left) 20 July and (right) 21 July. For OH the high-NO<sub>x</sub> and low-NO<sub>x</sub> regimes are shown separately.  $HO_2$  and  $RO_2$  for  $NO_x > 10$  ppb are not shown (below detection limits of MIESR and LIF). The solid lines represent linear fits with the indicated slopes.

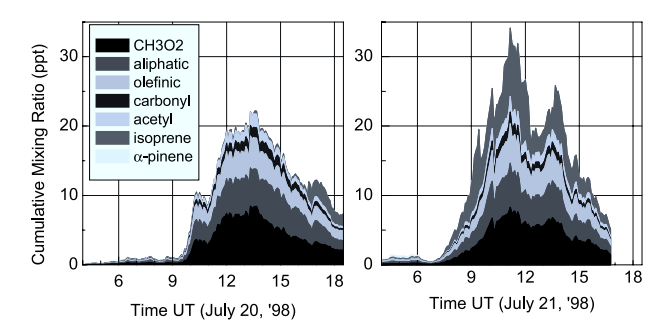


**Figure 3.** Speciation of  $RO_2$  as calculated by the MCM for (left) 20 July and (right) 21 July. See color version of this figure at back of this issue.

ratio on that day [cf., Konrad et al., 2003]. These authors show that isoprene predominated the total hydrocarbon reactivity on 21 July. A possible suggestion is therefore, that the chemical mechanism implemented in MCM significantly overestimates the peroxy radical production from isoprene oxidation.

#### 5. Discussion

#### 5.1. Radical Budgets

[30] Figures 4a and 4b show the major rates of production and destruction for the different radicals. The reactions that are taken into account are listed in Table 2. The rates were calculated from the measured values of the radicals, trace gases, and the photolysis frequencies, using the same rate coefficients as used in MCM. In general the rates of the recycling reactions which interconvert OH, HO<sub>2</sub>, and RO<sub>2</sub> are much faster than those of the primary production by photolysis of O<sub>3</sub>, HONO, and HCHO, or radical loss by radical-radical recombination. Only during the early morning, the OH is budget strongly influenced by the primary production via photolysis of HONO and O<sub>3</sub>, and destruction by the reaction of OH with NO<sub>2</sub>.

[31] The major OH production term is due to recycling reaction of HO<sub>2</sub> + NO (about 70%). The remaining OH production is associated to photolysis of O<sub>3</sub>. During the high-NO<sub>x</sub> period, destruction of OH with NO<sub>2</sub> and VOC are about equal, followed by the reaction with CO. In the low NO<sub>x</sub> period, reactions with VOC predominate the OH loss. On 21 July the OH destruction rate by VOCs is larger and more variable as on the previous day because of the much higher concentrations of isoprene, most likely due to nearby emissions.

[32] The major  $HO_2$  production term during the low  $NO_x$  period is the reaction of  $RO_2$  with NO (about 60%), followed by reactions of OH with CO and  $CH_2O$ , as well as photolysis of  $CH_2O$ . Photolysis of the higher aldehydes and ketones contributes only a few percent. Destruction of  $HO_2$  is mainly caused by reaction with NO (>80%). For high- $NO_x$  conditions an estimate production and destruction rates is difficult since the measured  $HO_2$  and  $RO_2$  concentrations are below the detection limit.

[33] The peroxy radical budget is dominated by reactions of OH with VOCs (50–70%), followed by production of  $CH_3O_2$  due to PAN decomposition (term P in equation (16)). In the afternoon of 21 July the net PAN decom-

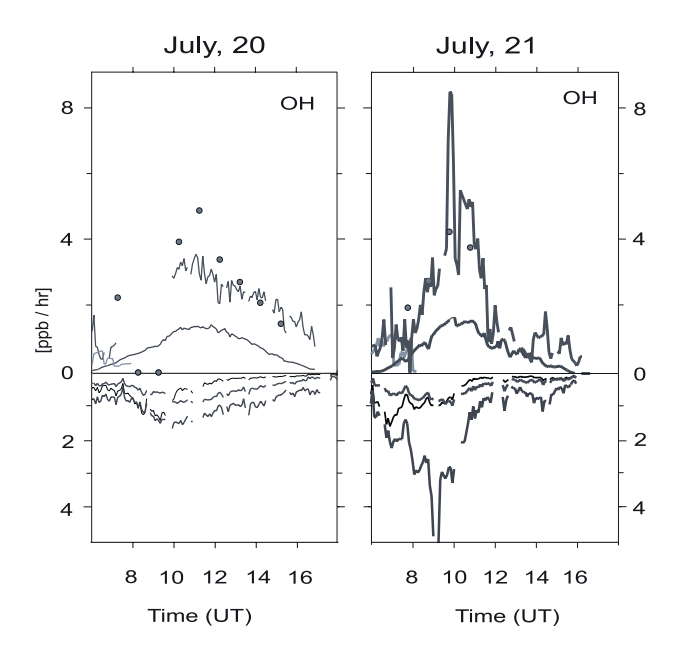


**Figure 4a.** Major production and destruction rates of OH during (left) 20 July and (right) 21 July calculated from the observations. OH:  $k_2 \times HO_2 \times NO$  (green line: LIF, gray circles: MIESR);  $k_1 \times H_2O \times O(^1D)$  (pink line); J(HONO)  $\times$  HONO (yellow line); OH destruction:  $k_8 \times OH \times NO_2$  (black line);  $k_i \times OH \times VOC_i$  (red line);  $k_3 \times OH \times CO$  (brown line). All values are in units of ppb/hr. See color version of this figure at back of this issue.

position equals the production rate by OH + VOC. Destruction of the  $RO_2$  radicals is always dominated by reaction with NO. Reactions of  $RO_2$  radicals with  $HO_2$  comprise a minor contribution, except for the MIESR sample collected around noon on 21 July. The gross destruction rate by reaction of  $RO_2$  with NO reaches 3.5 ppb/hr two times larger than the total  $RO_2$  production rate on 20 July. The  $RO_2$  destruction and production rates on 21 July are reasonably balanced.

[34] The ratios between the total production and destruction rates (P/D) of OH, HO<sub>2</sub> and RO<sub>2</sub> are shown in Figure 5. The data are shown only for the low NO<sub>x</sub> regime, where the MIESR measurements were significantly above the detection limit. In case of OH and HO2 it is found that the total production rates are generally larger than the total destruction rates. The ratio P/D for RO<sub>2</sub> is quite different for the two days. On 20 July the RO<sub>2</sub> production is considerable smaller than destruction, except for the last measured point. On 21 July the ratio P/D varies between 0.7 to 1.7. We note, however, that recycling of RO<sub>2</sub> from RO decomposition and isomerisation is missing in the RO<sub>2</sub> budgets. The contribution is difficult to calculate, as is described in section 3.2. In order to estimate its influence, MCM model results are used to correct the ratio P/D which is then shifted to net production (1 < P/D < 2.3) on both days.

[35] The budget of  $HO_2$  is governed by production from  $RO_2$  + NO and destruction by  $HO_2$  + NO (Figures 4a and 4b). The destruction and production terms are in balance within 10% on 20 July (Figure 5, middle), whereas production exceeds destruction by up to a factor of 1.6 on 21 July (Figure 5, middle).

[36] OH production exceeds destruction by up to a factors of 2 and 3 on 20 and 21 July, respectively (Figure 5). Production of OH is mainly due to reaction of HO<sub>2</sub> with NO during these periods (Figures 4a and 4b). The two independent HO<sub>2</sub> measurements (LIF and MIESR) agreed within 10%. The accuracy of the NO measurements is estimated to 5% [Volz-Thomas et al., 2003a, 2003b]. Likewise, the parameters used to calculate the OH production from ozone photolysis have accuracies of 5% for O<sub>3</sub>, H<sub>2</sub>O and 14% for J(O¹D). Therefore, the imbalance is unlikely caused by an overestimation of the production terms, but points to a missing sink for OH. This imbalance in the OH budget is in agreement with the overprediction of OH by the model (Figure 1), which forces a balanced budget.

[37] Overprediction of OH by constrained models was observed in a number of studies [McKeen et al., 1997; Hauglustaine et al., 1999; George et al., 1999; Carslaw et al., 1999] and several mechanisms, i.e. missing VOC reactivity and heterogeneous losses of OH and/or HO<sub>2</sub> on particles, were discussed as possible solutions for the observed discrepancy. In order to balance the OH production rates for 20 and 21 July an additional reactivity of 250–300 ppt isoprene equivalents is required (0.6–0.75 s<sup>-1</sup>). Such an additional amount of VOC reactivity would lead to a corresponding increase in the production of RO<sub>2</sub>. Likewise, including such a reactivity in the MCM leads to an

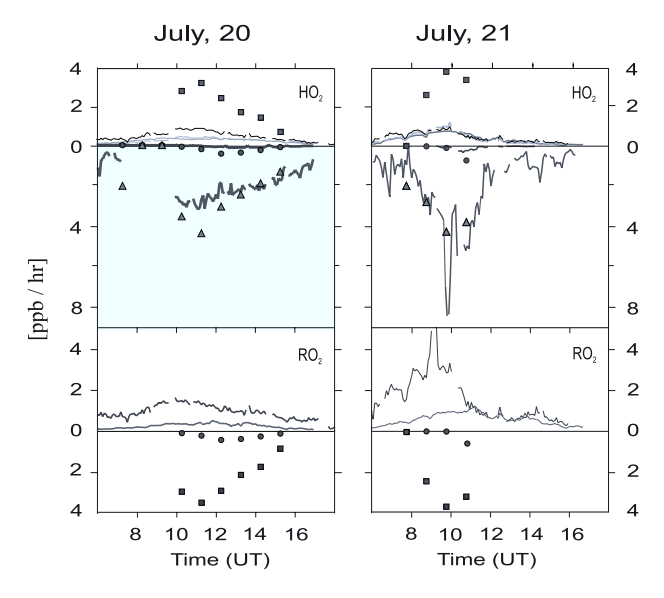


**Figure 4b.** Major production and destruction rates of HO<sub>2</sub> and RO<sub>2</sub> during (left) 20 July and (right) 21 July calculated from the observations. (top) HO<sub>2</sub>:  $k_5 \times RO_2 \times NO$  (blue squares);  $k_3 \times OH \times CO$  (black line);  $k_4 \times OH \times HCHO$  (yellow line); 2J(HCHO)<sub>radical</sub>  $\times$  HCHO (gray line); HO<sub>2</sub> destruction:  $k_2 \times HO_2 \times NO$  (green line, LIF) and pink triangles (MIESR);  $k_{10} \times HO_2 \times RO_2$  (brown circles, MIESR);  $k_9 \times HO_2 \times HO_2$  (red line, LIF). (bottom) RO<sub>2</sub>:  $k_i \times OH \times VOC_i + k_7 \times OH \times CH_4$  (red line); CH<sub>3</sub>O<sub>2</sub> production from PAN decomposition (blue line); RO<sub>2</sub> Destruction:  $k_5 \times RO_2 \times NO$  (green squares);  $k_{10} \times HO_2 \times RO_2$  (brown circles, MIESR). All values are in units of ppb/hr. See color version of this figure at back of this issue.

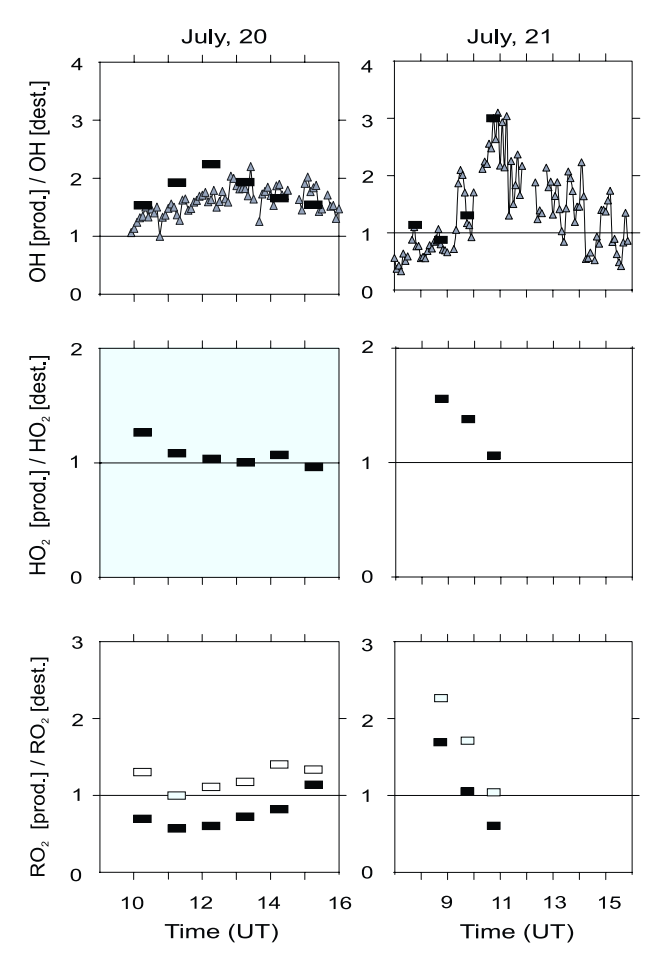


**Figure 5.** Diurnal variation of the ratio of total production and destruction rates for the different radicals on (left) 20 July and (right) 21 July for (top) OH (triangles from LIF data, rectangles from MIESR data), (middle) HO<sub>2</sub> (from MIESR data), and (bottom) RO<sub>2</sub> (from MIESR data, solid rectangles without RO chemistry, open rectangles including RO chemistry).

overestimation of the RO<sub>2</sub> mixing ratio by almost a factor of two. As a consequence, one would have to invoke VOCs or some other unknown species that do not produce RO<sub>2</sub> radicals upon oxidation by OH.

[38] The potential influence of heterogeneous radical losses on the budgets of OH, HO<sub>2</sub> and RO<sub>2</sub> was investigated in several studies [Cantrell et al., 1996; Saylor, 1997; Jacob, 2000; Kanaya et al., 2000]. At first approximation, the loss rates can be estimated from the specific surface area (A) of the particles and an uptake coefficient equation [cf., Carslaw et al., 1997]:

$$k = \gamma \times (RT/2\pi)^{0.5} {\times} A \tag{19} \label{eq:19}$$

The specific surface area A  $(m^2/m^3)$  was measured on both days with maximum values of  $220 \times 10^{-6}$   $(m^2/m^3)$  on 20 July and  $450 \times 10^{-6}$   $(m^2/m^3)$  on 21 July (Alicke, personal communication, 1999). The uptake coefficient for HO<sub>2</sub> was found to be  $\gamma > 0.025$  on ice and  $\gamma > 0.07$  on sulphuric acid (28%). For CH<sub>3</sub>C(O)O<sub>2</sub>,  $\gamma$  was found to be even smaller,  $\sim 0.004$  on water and  $\sim 0.001$  on sulphuric acid (51%)

[DeMore et al., 1997]. With these values for  $\gamma$ , there was little difference (<5%) in the modeled OH, HO<sub>2</sub> and RO<sub>2</sub> concentrations. In order to match the measured radical concentrations on 20 July an uptake coefficient of 0.5 is needed for both HO<sub>2</sub> and RO<sub>2</sub>, similar to the value used by Cantrell et al. [1996]. For 21 July, reasonable agreement within 20% is achieved for the OH concentration. The modeled HO<sub>2</sub> and RO<sub>2</sub> concentration are reduced by 20%, thus the overprediction remains high and is not resolved by including heterogeneous losses.

[39] A significant difference between the two days is the larger role of PAN in the RO<sub>2</sub> budget on 21 July because of slightly higher concentrations and the higher temperature. We have investigated the sensitivity of MCM to PAN by setting its concentration to zero. This extreme case scenario reduced the models overprediction of RO<sub>2</sub> on 21 July by about 20% and had practically no influence on the RO<sub>2</sub> concentrations on 20 July. Therefore errors in the rate coefficients for PAN decomposition or formation are unlikely the reason for the discrepancy in the RO<sub>2</sub> budget on 21 July.

#### 5.2. HO<sub>2</sub>/OH Ratios

[40] The discussion of the radical budgets has shown that the production and destruction of OH, HO<sub>2</sub>, and RO<sub>2</sub> is dominated by the reactions which convert these radicals into each other. Accordingly, the HO<sub>2</sub>/OH ratio would be expected to be controlled by the interconversion reactions as estimated by the simple steady state expression in reaction (16). The result of this simple model is plotted in panel F of Figure 1 (left and right) (dotted lines) and can be compared to the full MCM model calculation (solid lines). On both days the simple equation and the complex MCM model yield very similar results. The model predictions are in general good agreement with the observed HO<sub>2</sub>/OH ratio on 20 July, which suggests that the interconversion reactions for OH and HO2 are sufficiently well understood on this day. This is apparently not the case on the other day, 21 July, where the MCM and the simple model both fail to reproduce the observed variability of HO<sub>2</sub>/OH. The variance is most likely due to strong fluctuations in the concentrations of isoprene and other biogenic VOCs that are advected from the nearby forest. These variations are not resolved by the gas chromatographic measurements which represent 20 min averages [Konrad et al., 2003]. The apparent discrepancy between model and radical concentrations thus highlights the need for time resolved VOC measurements in situations, where close by sources cannot be ruled out. Quite different results have been reported recently by Tan et al. [2001] for an environment, where much higher isoprene concentrations (several ppb) were present. In the PROPHET campaign they measured OH and HO<sub>2</sub> inside a deciduous forest at low NO<sub>x</sub> (<1ppb) for low NO<sub>x</sub> conditions. For the modeled HO<sub>2</sub> they found good agreement with the observations, whereas the model was generally unable to match the measured OH, with the observations 2.7 times greater than the model on average. As a result, the modeled  $HO_2/OH$  ratios were 2.5–4 times higher than the measured ratios, indicating that the cycling between OH and HO<sub>2</sub> was poorly described by the model [Tan et al., 2001]. The results from PROPHET and BER-LIOZ suggest that biogenic VOC possibly have a complex

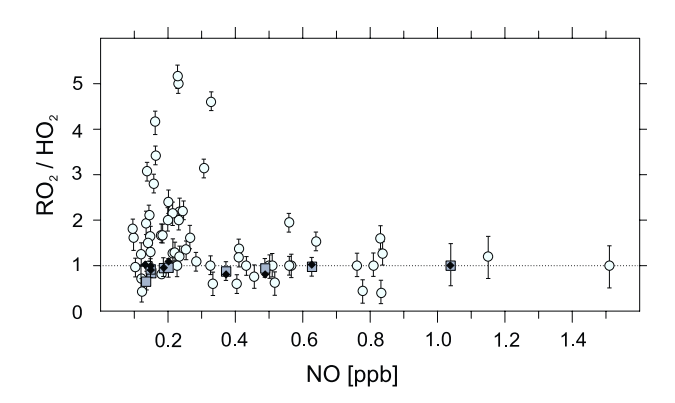


**Figure 6.** Ratios of  $RO_2$  to hydroperoxy radicals for different NO concentrations measured by MIESR during field campaigns in 1989, 1990, 1992 and 1994 at Schauinsland (open circles) and during BERLIOZ (measurements shaded square, and solid diamonds, MCM calculations). The data represent half hourly values and are filtered for  $J(NO_2) \geq 0.004~{\rm s}^{-1}$ .

influence on the tropospheric photochemical system which is not yet well understood.

### 5.3. RO<sub>2</sub>/HO<sub>2</sub> Ratios

[41] Figure 6 shows the dependence of RO<sub>2</sub>/HO<sub>2</sub> as measured at Pabstthum with those obtained during several previous campaigns at Schauinsland in the Black Forest, Germany, as a function of the prevailing NO mixing ratio. Moreover, the MCM model predictions for Pabstthum are included in the Figure 6. The data are selected for J(NO<sub>2</sub>)  $> 0.004 \text{ s}^{-1}$ . The measurements at Schauinsland show RO<sub>2</sub>/HO<sub>2</sub> ratios of up to 5 at low NO concentrations. The ratio declines rapidly at NO > 0.3 ppb to a value of around 1. Note that the RO2 and HO2 concentrations are near to or below the detection limit of the MIESR for NO > 1.6 ppb. For the conditions at Pabstthum the MCM predicts RO<sub>2</sub>/HO<sub>2</sub> ratios of about one, almost independent of the NO mixing ratio between 0.05 and 10 ppb in excellent agreement with the MIESR data. The simple steady state model (reaction (17)) predicts much lower ratios since it does not account for RO2 recycling from the decomposition and isomerisation of the alkoxy radicals. Obviously, MCM describes most of these processes correctly.

[42] Stevens et al. [1997] discuss  $RO_2/HO_2$  ratios for the TOPHE campaign at Idaho Hill which were derived from the combination of CA data ( $RO_2 + HO_2$ ) and  $HO_2$  measurements by LIF. They find ratios of about 4–5 under clean conditions (NO < 0.2 ppb) in good agreement with the data from Schauinsland. The model used by Stevens et al. [1997] predicts a  $RO_2/HO_2$  ratio of about one, in agreement with the MCM results for Pabstthum. It seems therefore that the current chemical mechanisms miss an important process that leads to higher  $RO_2/HO_2$  ratios at low  $NO_x$  concentrations.

[43] Under polluted conditions (NO > 1.5 ppb), however, these authors find  $RO_2/HO_2$  ratios of 12–14, much higher than what is observed at either Pabstthum or Schauinsland. The very large  $RO_2/HO_2$  ratios observed by *Stevens et al.* 

[1997] in the presence of 1.6–1.9 ppb NO are almost exclusively due the very high RO<sub>2</sub> + HO<sub>2</sub> concentrations (5-11 ppt) measured by the chemical amplifier [Cantrell et al., 1997]. The coexistence of such high RO2 and NO mixing ratios is impossible to explain with our current understanding of the radical chemistry and disagrees with MIESR measurements from several campaigns. Stevens et al. [1997] discuss two possible solutions for the discrepancy between the model and their measurements: A 10 times smaller value for the rate coefficient of reaction (5) RO<sub>2</sub> + NO and a factor of 5 larger rate coefficients for the recombination reactions of RO2 with HO2. The major improvement comes from reaction (5), since the peroxy radical recombination has little influence on the RO<sub>2</sub>/HO<sub>2</sub> ratio except for conditions where NO<sub>x</sub> is extremely low. The VOC reactivity at Idaho Hill under high-NO<sub>x</sub> conditions is dominated by isoprene of ( $\sim 2.1 \text{ s}^{-1}$ ), followed by ethene ( $\sim 1 \text{ s}^{-1}$ ), propene ( $\sim 1 \text{ s}^{-1}$ ) and HCHO of  $(\sim 0.65 \text{ s}^{-1})$ . It is difficult to believe that the RO<sub>2</sub> radicals, produced by oxidation of these hydrocarbons, would react 10 times more slowly than recommended by Atkinson [1997]. For example, the measured rate constants for the hydroxyalkyl peroxy radicals  $HOCH_2CH_2O_2$  (9 ×  $10^{-12}$ cm<sup>3</sup> s<sup>-1</sup> [Le Bras, 1997]) and OHC(CH<sub>3</sub>)<sub>2</sub>CCH<sub>2</sub>O<sub>2</sub> (4.9 ×  $10^{-12}$  cm<sup>3</sup> s<sup>-1</sup> [Wallington et al., 1997]) are within a factor 2 of the recommendation for the corresponding alkyl peroxy radicals [Atkinson, 2000]. Also, a 10 times smaller rate coefficient for RO<sub>2</sub> + NO would lead to even larger discrepancies for the NO/NO2 ratio derived from the direct measurements and from the photostationary state (PSS) (see discussion by Volz-Thomas et al. [2003b]).

[44] Aerosol formation during the photooxidation of biogenic VOC would be another possible reason for decreasing the  $HO_2$  production from the initial  $RO_2$  radicals. The yield of aerosol formation was measured by *Pandis et al.* [1991] for several compounds and ranged from negligible in the case of isoprene, 30–40% for  $\beta$ -pinene and limonene, to 100% for trans-caryophyllene. *Hoffmann et al.* [1997] note, however, that ozonolysis is responsible for most of the aerosol formation in the oxidation of the biogenic monoterpenes and sesquiterpenes in their studies.

### 6. Ozone Production Rates

[45] It is generally assumed [cf., *Volz et al.*, 1988; *Ridley et al.*, 1992; *Kleinman et al.*, 1995; *Frost et al.*, 1998] that the photochemical ozone formation rate  $P(O_3)$  is approximately determined by the rate at which NO is oxidized to  $NO_2$  by reaction with peroxy radicals ( $HO_2$  and  $RO_2$  (see reactions (2) and (5) in Table 2). In this approach, the minor pathway of the higher organic peroxy radicals that leads to formation of organic nitrates and the loss of  $NO_2$  by reaction with OH are neglected. In this respect reaction (20) represents an upper limit for  $P(O_3)$ .

$$\begin{split} P(O_3) &= [NO] \times \left\{ k_2 [HO_2] + \Sigma \left( k_{5i} [RO_2]_i \right) \right\} \\ &\cong [NO] \times \left\{ k_2 [HO_2] + k_5 [RO_2] \right\} \end{split} \tag{20} \end{split}$$

The ozone production rate data for Pabstthum on 20 and 21 July are shown in Figure 7 as a function of NO,

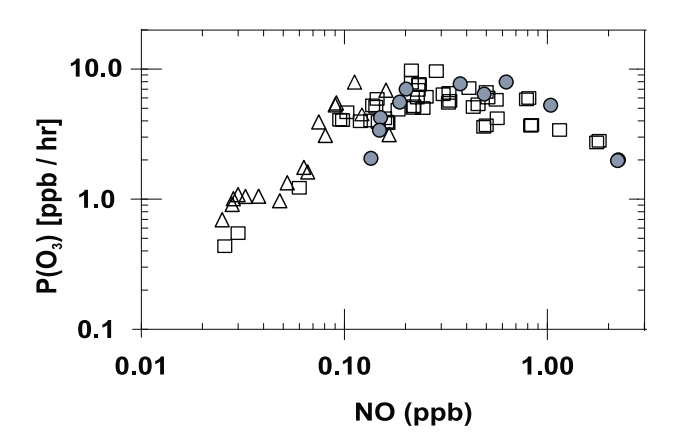


**Figure 7.** Comparison of the ozone production rate calculated from the measured radical concentrations (reaction 20) during the BERLIOZ campaign (solid circles) to those calculated from the MIESR measurements made during several campaigns at Schauinsland (summer 1989, 1990, 1992 and 1994, squares) and in August 1993 at Izana, Tenerife (triangles). The simultaneously observed NO mixing ratio is used as abscissa. The data represent half hourly values and are filtered for  $J(NO_2) \geq 0.004 \ s^{-1}$ .

denoted by the filled circles. Note that both scales are logarithmic. Also shown are values for  $P(O_3)$  obtained from earlier campaigns at Schauinsland (1989, 1990, 1992, 1994) and Tenerife [1995]. In each case,  $P(O_3)$  was calculated from the peroxy radical concentrations measured by MIESR and the average NO concentration in the MIESR sampling period data and selected for  $J(NO_2) > 0.004 \, s^{-1}$ . An average rate coefficient of  $k_5 = 8.6 \times 10^{-12} \, cm^3 \, s^{-1}$  for the reaction of organic peroxy radicals with NO was estimated from the evaluation of the different rate coefficients by [Atkinson, 1997] and the partitioning of the radicals provided by MCM. For  $HO_2$ , the rate coefficient by Bohn and Zetzsch [1997] was used.

[46] The observed O<sub>3</sub> production rate at Pabstthum shows a strong increase with the NO mixing ratio between 0.1 and 0.3 ppb, where  $P(O_3)$  reaches a maximum value of 8 ppb/hr. The dependence of P(O<sub>3</sub>) on NO at concentrations below 0.3 ppb has a positive slope of 53 ppb/hr per ppb NO. Above 0.5 ppb NO the rate of ozone production decreases linearly with a slope of 3.3 (ppb/hr)/(ppb NO). This behavior can be compared with the P(O<sub>3</sub>) data obtained from Schauinsland and Tenerife. The corresponding peroxy radical and NO measurements at Schauinsland were made in May 1989, August 1990, September 1992, and August 1994. [Mihelcic and Volz-Thomas, 1994]. At Izana, Tenerife, measurements were performed during the OCTA (Oxidizing Capacity of the Tropospheric Atmosphere) intensive in August 1993 [Schultz, 1995; Fischer et al., 1998; Zenker et al., 1998]. The P(O<sub>3</sub>) data from these campaigns show a similar behavior as was observed at Pabstthum. A strong, nearly linear increase with the NO mixing ratio is found between 0.02 and 0.25 ppb, where P(O<sub>3</sub>) reaches a maximum value of 10 ppb/hr. At NO values above 0.3 ppb, P(O<sub>3</sub>) decreases slowly with further increasing NO concentrations. The linear increase below 0.3 ppb NO has a slope that is about 30% smaller than observed during the BER-LIOZ campaign, whereas the decreasing trend of  $P(O_3)$  above 0.5 ppb NO is very similar to what is found at Pabstthum. The scatter of the  $P(O_3)$  data over the whole range of the NO mixing ratios is relatively low, suggesting some similarity of the ozone production for the three different places in Europe.

[47] A similar dependence of the ozone production rate on the NO concentration was calculated using a steady photochemical model by *Kleinman et al.* [2000]. The calculated P(O<sub>3</sub>) show a maximum value of up to 11 ppb/hr, and shows nearly linear dependence of P(O<sub>3</sub>) on NO, at NO concentrations below 0.25 ppb [*Kleinman et al.*, 2000]. *Frost et al.* [1998] investigated the dependence of the ozone production on NO<sub>x</sub>. They found a slope for low [NO<sub>x</sub>] (<2 ppb) of about 6 [ppb/hr]/[ppb NO<sub>x</sub>]. This is in the same order of magnitude as our observation of about 7 [ppb/hr]/[ppb NO<sub>x</sub>]. Nevertheless, their maximum value of ozone production, calculated from [RO<sub>x</sub>] measurements by chemical amplifier techniques [*Cantrell et al.*, 1992, 1993] was about a factor of 4 higher than ours, because of the higher isoprene concentrations during the ROSE campaign.

# 7. Summary and Conclusions

[48] In this paper we have analyzed radical measurements of OH,  $\mathrm{HO}_2$ , and  $\mathrm{RO}_2$ , which were obtained in a rural environment near the city of Berlin on two intensive days (20 and 21 July) in summer 1998. On both days the atmospheric conditions were characterized by high- $\mathrm{NO}_x$  levels (10–30 ppb) in the morning, followed by a transition to relatively low  $\mathrm{NO}_x$  concentrations, which were about an order of magnitude smaller and persisted until the evening. The two days were distinctly different with respect to the chemical composition of the VOC. On 21 July high isoprene levels were encountered, indicating the advection of biogenic VOC emissions from a nearby mixed forest.

[49] The concentrations and diurnal variations of the radicals showed a similar behavior for the two days. Relatively high OH concentrations of  $(2-4)\times 10^6~{\rm cm}^{-3}$  were observed at high  $NO_x$  in the morning, while  $HO_2$  and  $RO_2$  remained near the detection limit ( $\sim\!1-2$  ppt) for these conditions. At low  $NO_x$  the concentrations of OH reached  $(6-8)\times 10^6~{\rm cm}^{-3}$  at local noon, while  $HO_2$  and  $RO_2$  reached 20-30 ppt, each. The  $HO_2/OH$  ratio varied from 10 to 240, with higher values observed at low  $NO_x$ . The  $RO_2/HO_2$  ratio was quite constant and showed values between  $\sim\!0.75$  and 1.0 during daytime.

[50] The observed radical concentrations and their ratios have been compared with model simulations using a Master Chemical Mechanism (MCM) that was constrained by measured values of a comprehensive suite of trace gases and photolysis frequencies. Main features of the diurnal radical cycles are reasonably reproduced by the model, for example the strong increase of the radicals during the transition from high- to low-NO<sub>x</sub> conditions. At high NO<sub>x</sub> the concentration of OH is well described by the model with only slight overpredictions ( $\sim$ 10% on July 20,  $\sim$ 30% on 21 July). The analysis of the radical budget has shown that in this case OH was strongly

influenced by the primary production via photolysis of HONO and  $O_3$ , and the destruction of OH via the reaction with  $NO_2$ . For the peroxy radicals the model predictions agree with the observed low concentration values. A precise comparison is not possible in this case, because the peroxy radical measurements were at the detection limit.

- [51] At low NO<sub>x</sub> the model generally tends to overestimate all radicals (OH, HO<sub>2</sub>, RO<sub>2</sub>) by varying amounts. OH is overpredicted by a factor of 1.5-1.7 on the two days. In case of the peroxy radicals the overprediction on July 21 is larger than on the previous day, reaching a factor of 2 or more, when isoprene concentrations were high. In general the ratios HO<sub>2</sub>/OH and RO<sub>2</sub>/HO<sub>2</sub> are much better reproduced by the model than the individual measurements. On 20 July the modeled ratios agree within 20% with the observations. On the following day, the model fails to reproduce the large variability of the experimental HO<sub>2</sub>/OH ratio. The observed variance on this day was likely due to fluctuations of isoprene and other biogenic VOC from nearby sources, which were not resolved by the gas chromatographic measurements and therefore not appropriately considered in the model.
- [52] The analysis of the radical budgets has been performed almost completely on the basis of field observations. The analysis shows that the recycling reactions, which interconvert OH, HO<sub>2</sub>, and RO<sub>2</sub>, dominate the chemical turnover and the ratios of the radicals under the conditions of BERLIOZ at NO<sub>x</sub> levels below 10 ppb. Thus, the agreement of the modeled and observed ratios HO2/OH and RO<sub>2</sub>/HO<sub>2</sub> demonstrates that the radical recycling is reasonably well described by the model, at least for the conditions on 20 July. The measured radical ratios have also been compared with the result of a simple steady state model, which only accounts for cycling reactions of the radicals. The simple model reproduces the observed HO<sub>2</sub>/ OH ratio as well as the complex MCM model, but underestimates the RO<sub>2</sub>/HO<sub>2</sub> ratio by a factor 1.2–1.8. This factor reflects the efficiency of the neglected RO<sub>2</sub> recycling from the decomposition and isomerisation of the alkoxy radicals. Apparently the MCM model accounts for most of these processes correctly.
- [53] The general model overprediction of the radicals at low NO<sub>x</sub> is consistent with the empirical radical budgets, which show that the total production rates are larger than the total destruction rates for this condition. Since there is no experimental evidence that the production rates are determined too high, the budgets can only be balanced by additional radical sinks, which do not recycle OH, HO<sub>2</sub>, or RO<sub>2</sub>. No process could be identified that would quantitatively explain this kind of radical loss. Missing VOC in the model could be responsible for the overprediction of OH, but would not explain the overprediction of HO2 and  $RO_2$ . Loss of OH by the reaction with HX (X = Br, I) would lower the radical concentrations, but unreasonably high HX concentrations in the order of one ppb would be required to explain the observed OH. Heterogeneous loss processes on aerosol can be ruled out as an unlikely explanation, since an uptake coefficient of about 0.5 would be needed, which is much larger than laboratory measurements suggest.

- [54] The measured peroxy radicals have been used to estimate the local ozone production rate during BERLIOZ. The production rate was found to increase linearly with NO below 0.3 ppb NO and to decrease above 0.5 ppb NO. The maximum rate of 8 ppb/hr was encountered at 0.3 ppb NO. A similar behavior of the ozone production rate has been derived from previous peroxy radical measurements at Schauinsland in the Black Forest and Tenerife, where the maximum  $\rm O_3$  production never exceeded values of 10 ppb/hr.
- [55] In conclusion, the comprehensive data set of radical measurements at BERLIOZ has given interesting insight into the photochemistry of the lower troposphere and has confirmed important aspects in the tropospheric master chemical mechanism. There remain, however, significant deficiencies in the model, such as the model overprediction of the radicals, for which no conclusive explanation has been found. The role of biogenic VOC as a sink of OH and source of peroxy radicals requires more attention. In this respect, the development of faster VOC measurement techniques with a time resolution of about a few minutes would support greatly future field studies of the fast radical photochemistry.
- [56] **Acknowledgments.** We gratefully acknowledge the financial support by the German Minister for Research and Development (BMFT) as part of the Tropospheric Research Focus (TFS), Theme 3 under grant no. 07TFS 31/HA.3, and of EUROTRAC-TOR (grant 07 EU 723). The measurements at Tenerife were kindly supported by the European Commission, DG-XII as part of the project OCTA (EV5V-CT91-0042). We are especially grateful and thank Andreas Wahner and Dieter Klemp for helful discussions.

#### References

- Alicke, B., A. Geyer, A. Hofzumahaus, F. Holland, S. Konrad, H. W. Pätz, J. Schäfer, J. Stutz, A. Volz-Thomas, and U. Platt, OH formation by HONO photolysis during the BERLIOZ experiment, J. Geophys. Res., 108(D4), 8247, doi:10.1029/2001JD000579, 2003.
- Atkinson, R., Gas-phase tropospheric chemistry of volatile organic compounds: Alkanes and alkenes, *J. Phys. Chem. Ref. Data*, 26(2), 1997
- Atkinson, R., Atmospheric chemistry of VOCs and NO<sub>x</sub>, *Atmos. Envinron.*, 34, 2063–2101, 2000.
- Bohn, B., and C. Zetzsch, Rate constant of HO<sub>2</sub> + NO covering atmospheric conditions, 1, HO<sub>2</sub> formed by OH + H<sub>2</sub>O<sub>2</sub>, *J. Phys. Chem.*, 101, 1488–1493, 1997.
- Brauers, T., M. Hausmann, A. Bister, A. Kraus, and H. P. Dorn, OH radicals in the boundary layer of the Atlantic Ocean, 1, Measurements by long-path laser absorption spectroscopy, *J. Geophys. Res.*, 106, 7399–7414, 2001.
- Cantrell, C. A., et al., Peroxy radicals in the ROSE Experiment: Measurement and theory, J. Geophys. Res., 97, 20,671–20,686, 1992.
- Cantrell, C. A., et al., Peroxy radicals as measured in ROSE and estimated from photostationary state deviations, *J. Geophys. Res.*, 98, 18,355–18,366, 1993.
- Cantrell, C. A., R. E. Shetter, T. M. Gilpin, J. G. Calvert, F. L. Eisele, and D. J. Tanner, Peroxy radical concentration measured and calculated from trace gas measurements in the Mauna Loa Observatory Photochemistry Experiment 2, *J. Geophys. Res.*, 101, 14,653–14,664, 1996.
- Cantrell, C. A., R. E. Shetter, J. G. Calvert, F. L. Eisele, E. Williams, K. Baumann, W. H. Brune, P. S. Stevens, and J. H. Mather, Peroxy radicals from photostationary state deviations and steady state calculations during the tropospheric OH photochemistry experiment at Idaho Hill, Colorado, 1993, J. Geophys. Res., 102, 6369–6378, 1997.
- Carroll, M. N., P. B. Shepson, and S. B. Bertman, Overview of the Program for Research on Oxidants: Photochemistry, Emissions, and Transport (PROPHET) summer 1998 measurements intensive, *J. Geophys. Res.*, 106, 24,275–24,288, 2001.
- Carslaw, N., L. J. Carpenter, J. M. C. Plane, B. J. Allan, R. A. Burgess, K. C. Clemitshaw, H. Coe, and S. A. Penkett, Simultaneous observations of

- nitrate and peroxy radicals in the marine boundary layer, J. Geophys. Res., 102, 18,917-18,933, 1997
- Carslaw, N., D. J. Creasey, D. E. Heard, A. C. Lewis, J. B. McQuaid, M. J. Pilling, P. S. Monks, B. J. Bandy, and S. A. Penkett, Modeling OH, HO2 and RO<sub>2</sub> radicals in the marine boundary layer, 1, Model construction and comparison with field measurements, J. Geophys. Res., 104, 30,241-30,255, 1999.
- Chameides, W. L., and J. G. Walker, A photochemical theory of tropospheric ozone, J. Geophys. Res., 78, 8751-8760, 1973.
- Chen, G., et al., An investigation of South Pole HO<sub>x</sub> chemistry: Comparison of model results with ISCAT observation, Geophys. Res. Lett., 28, 3633-3636, 2001.
- Crutzen, P. J., The role of NO and NO2 in the chemistry of the troposphere and stratosphere, Annu. Rev. Earth. Planet. Sci., 7, 443-472, 1979.
- Curtis, A. R., and W. P. Sweetenham, FACSIMILE/CHEKMAT users manual, Rep. AERER12805, Her Majesty's Stn. Off., Norwich, UK,
- DeMore, W. B., S. P. Sander, D. M. Golden, R. F. Hampson, M. J. Kurylo, C. J. Howard, A. R. Ravishankara, C. E. Kolb, and M. J. Molina, Chemical kinetics and photochemical data for use in stratospheric modeling, Evaluation Number 12, JPL Publication 97-4, Jet Propulsion Lab., Calif. Inst. of Technol., Pasadena, Calif., 1997.
- Ehhalt, D. H., Photooxidation of trace gases in the troposphere: Plenary lecture, *Phys. Chem. Chem. Phys.*, *1*, 5401–5408, 1999.
- Ehhalt, D. H., H.-P. Dorn, and D. Poppe, The chemistry of the hydroxyl radical in the troposphere, Trans. R. Soc. Edinburgh, 97, 17-34, 1991.
- Fischer, H., et al., Trace gas measurements during the Oxidizing Capacity of the Tropospheric Atmosphere campaign 1993 Izaña, J. Geophys. Res., 103, 13,505-13,518, 1998
- Frost, G. J., et al., Photochemical ozone production in the rural southeastern United States during the 1990 Rural Oxidants in the Southern Environment (ROSE) program, J. Geophys. Res., 103, 22,491-22,508,
- George, L. A., T. M. Hard, and R. J. O'Brien, Measurement of free radicals OH and HO<sub>2</sub> in Los Angeles smog, J. Geophys. Res., 104, 11,643-11,655, 1999
- Geyer, A., B. Alicke, D. Mihelcic, J. Stutz, and U. Platt, Comparison of tropospheric NO<sub>3</sub> radical measurements by differential optical absorption spectroscopy and matrix isolation electron spin resonance, J. Geophys. Res., 104, 26,097-26,105, 1999.
- Geyer, A., et al., Nightime formation of peroxy and hydroxyl radicals during the BERLIOZ campaign: Observations and modeling studies, J. Geophys. Res., 108(D4), 8249, doi:10.1029/2001JD000656, 2003.
- Glaser, K., U. Vogt, G. Baumbach, A. Volz-Thomas, and H. Geiss, Vertical profiles of O<sub>3</sub>, NO<sub>2</sub>, NO<sub>x</sub>, VOC, and meteorological parameters during the Berlin Ozone Experiment (BERLIOZ) campaign, J. Geophys. Res., 108, doi:10.1029/2001JD002475, in press, 2003.
- Grossmann, D., et al., Hydrogen peroxide, organic peroxides, carbonyl compounds and organic acids measured at Pabstthum during BER-LIOZ, J. Geophys. Res., 108, doi:10.1029/2001JD001096, in press, 2003.
- Hauglustaine, D. A., S. Madronich, B. A. Ridley, S. J. Flocke, C. A. Cantrell, F. L. Eisele, R. E. Shetter, D. J. Tanner, P. Ginoux, and E. L. Atlas, Photochemistry and budget of ozone during the Mauna Loa Observatory Photochemistry Experiment (MLOPEX 2), J. Geophys. Res., 104, 30,275-30,307, 1999.
- Hoffmann, T., J. R. Odum, F. Bowman, D. Collins, D. Klockow, R. C. Flagan, and J. H. Seinfeld, Formation of organic aerosols from the oxidation of biogenic hydrocarbons, J. Atmos. Chem., 26, 189-222, 1997
- Holland, F., A. Hofzumahaus, J. Schäfer, A. Kraus, and H. W. Pätz, Measurements of OH and HO2 radical concentrations and photolysis frequencies during BERLIOZ, J. Geophys. Res., 108(D4), 8246, doi:10.1029/2001JD0001393, 2003.
- Jacob, D. J., Heterogeneous chemistry and tropospheric ozone, Atmos. Environ., 34, 2131-2159, 2000.
- Jefferson, A., D. J. Tanner, F. L. Eisele, D. D. Davis, G. Chen, J. Crawford, J. W. Huey, A. L. Torres, and H. Berresheim, OH photochemistry and methane sulfonic acid formation in the coastal Antartic boundary layer, J. Geophys. Res., 103, 1647-1656, 1998.
- Jenkin, M. E., S. M. Saunders, and M. J. Pilling, The tropospheric degradation of volatile organic compounds: A protocol for mechanism development, Atmos. Environ., 31, 81-104, 1997.
- Kanaya, Y., Y. Sadanaga, J. Matsumoto, U. K. Sharma, J. Hirokawa, Y. Kajii, and H. Akimoto, Daytime HO2 concentrations at Oki Island, Japan, in summer 1998: Comparison between measurement and theory, J. Geophys. Res., 105, 24,205-24,222, 2000.
- Kleinman, L., Y.-N. Lee, S. R. Springston, J. H. Lee, L. Nunnermacker, J. Weinstein-Lloyd, X. Zhou, and L. Newman, Peroxy radical concentration

- and ozone formation rate at a rural site in southeastern United States, J. Geophys. Res., 100, 7263-7273, 1995.
- Kleinman, L. I., P. H. Daum, D. G. Imre, J. H. Lee, Y.-N. Lee, L. J. Nunnermacker, S. R. Springston, J. Weinstein-Lloyd, and L. Newman, Ozone production in the New York City urban plume, J. Geophys. Res., 105, 14,495 – 14,511, 2000.
- Konrad, S., et al., Hydrocarbon measurements at Pabstthum during the BERLIOZ campaign and modeling of free radicals, J. Geophys. Res., 108, doi:10.1029/2001JD000866, in press, 2003.
- LeBras, G., Chemical processes in atmospheric oxidation, in Transport and Chemical Transformation of Pollutants in the Troposphere, edited by P. Borrell et al., Springer-Verlag, New York, 1997.
- Levy, H., II, Normal atmosphere: Large radical and formaldehyde concen-
- trations predicted, *Science*, 173, 141–143, 1971. Logan, J. A., M. J. Prather, S. C. Wofsy, and M. B. McElroy, Tropospheric chemistry: A global perspective, J. Geophys. Res., 86, 7210-7254,
- McKeen, S. A., et al., Photochemical modeling of hydroxyl and its relationship to other species during the Tropospheric OH Photochemistry Experiment, J. Geophys. Res., 102, 6467-6493, 1997.
- Mihelcic, D., and A. Volz-Thomas, The ratio of organic per-oxy to hydroperoxy radicals: Direct measurements by Matrix Isolation/ESR Spectroscopy, in Transport and Transformation of Pollutants in the Troposphere: EUROTRAC Symposium, edited by P. B. Borrell et al., pp. 379-384, SPB Acad., Garmisch-Partenkirchen, Germany, 1994.
- Mihelcic, D., P. Müsgen, and D. H. Ehhalt, An improved method of measuring tropospheric NO2 and RO2 by matrix isolation and electron spin resonance, J. Atmos. Chem., 3, 341-361, 1985.
- Mihelcic, D., A. Volz-Thomas, H. W. Pätz, D. Kley, and M. Mihelcic, Numerical analysis of ESR spectra from atmospheric samples, J. Atmos. Chem., 11, 271-297, 1990.
- Mount, G. H., and E. J. Williams, An overview of the Tropospheric OH Photochemistry Experiment, Fritz Peak/Idaho Hill, Colorado, Fall 1993, J. Geophys. Res., 102, 6171-6187, 1997.
- Pandis, S. N., S. E. Paulson, J. H. Seinfeld, and R. C. Flagan, Aerosol formation in the photooxidation of isoprene and  $\beta$ -pinene, Atmos. Envinron., Part A, 25, 997-1008, 1991.
- Poppe, D., et al., Comparison of measured OH concentrations with model calculation, *J. Geophys. Res.*, 99, 16,633–16,642, 1994. Ridley, B. A., S. Madronich, R. B. Chatfield, J. G. Walega, R. E. Shetter,
- M. A. Carroll, and D. D. Montzka, Measurements and model simulation of the photostationary state during the Mauna Loa Observatory photochemistry experiment: Implications for radical concentrations and ozone production and loss rates, J. Geophys. Res., 97, 10,375-10,388, 1992.
- Sander, S. P., et al., Chemical kinetics and photochemical data for use in stratospheric modeling, Evaluation 13, *JPL Publ.*, 00-3, 2000.
- Saylor, R. D., An estimate of the potential significance of heterogeneous loss aerosols as an additional sink for hydroperoxy radicals in the troposphere, Atmos. Environ., 31, 3653-3658, 1997.
- Schlomski, S., Development of analytical methods for the determination of carbonyl compounds in the atmosphere, Ph.D. thesis, TU Darmstadt, Darmstadt, Germany, 2000.
- Schultz, M., Die Bedeutung von Stickoxiden für die Ozonbilanz in Reinluftgebieten, Ph.D. thesis, Univ. of Wuppertal, Wuppertal, Germany,
- Stevens, P. S., et al., HO<sub>2</sub>/OH and RO<sub>2</sub>/HO<sub>2</sub> ratios during the tropospheric OH photochemistry experiment: Measurement and theory, J. Geophys. Res., 102, 6379-6391, 1997.
- Stockwell, W. R., F. Kirchner, M. Kuhn, and S. Seefeld, A new mechanism for regional atmospheric chemistry modelling, J. Geophys. Res., 102, 25,847-25,879, 1997.
- Tan, D., et al., HO<sub>x</sub> gets in a deciduous forest: Results from the PRO-PHET summer 1998 campaign, J. Geophys. Res., 106, 24,407-24,427,
- Tanner, D. J., A. Jefferson, and F. L. Eisele, Selected ion chemical ionization mass spectrometric measurement of OH, J. Geophys. Res., 102, 6415-6426, 1997.
- Trainer, M., E. Y. Hsie, S. A. McKeen, R. Tallamraju, D. D. Parrish, F. C. Fehsenfeld, and S. C. Liu, Impact of natural hydrocarbons on hydroxyl and peroxy radicals at a remote site, J. Geophys. Res, 92, 11,879-11,894,
- Volz, A., D. Mihelcic, P. Müsgen, H.-W. Pätz, G. Pilwat, H. Geiss, and D. Kley, Ozone production in the Black Forrest: Direct measurements of RO<sub>2</sub>, NO<sub>x</sub> and other relevant parameters, in Tropospheric Ozone: Regional and Global Scale Interactions, NATO ASI Ser., Ser. C, vol. 227, edited by I. S. A. Isaksen, pp. 293-302, D. Reidel, Norwell, Mass.,
- Volz-Thomas, A., H. Geiss, A. Hofzumahaus, and K.-H. Becker, Fast photochemistry experiment in BERLIOZ (PHOEBE): An introduc-

- tion, J. Geophys. Res., 108, doi:10.1029/2001JD002029, in press, 2003a.
- Volz-Thomas, A., H.-W. Pätz, N. Houben, S. Konrad, D. Mihelcic, T. Klüpfel, and D. Perner, Inorganic trace gases and peroxy radicals during BERLIOZ at Pabstthum: An investigation of the photostationary state (PSS) of NO<sub>x</sub> and O<sub>3</sub>, *J. Geophys. Res.*, 108(D4), 8248, doi:10.1029/2001JD001255, 2003b.
- Wallington, T. J., M. D. Herley, J. C. Ball, A. M. Straccia, J. Platz, L. K. Christensen, J. Sehested, and O. J. Nielsen, Atmospheric cyhemistry of dimethoxymethane (CH<sub>3</sub>OCH<sub>2</sub>OCH<sub>3</sub>): Kinetics and mechanism of its reaction with OH radicals and fate of the alkoxy radicals: CH<sub>3</sub>O-CH(O)OCH<sub>3</sub> and CH<sub>3</sub>OCH<sub>2</sub>OCH<sub>2</sub>(O), *J. Phys. Chem. A*, 101, 5302–5308, 1997.
- Zenker, T., et al., Intercomparison of NO,  $NO_2$ ,  $NO_y$ ,  $O_3$ , and  $RO_x$  measurements during the Oxidising Capacity of the Tropospheric Atmosphere

(OCTA) campaign 1993 at Izaňa, *J. Geophys. Res.*, 103, 13,615–13,634, 1998.

B. Alicke, A. Geyer, and U. Platt, Ruprecht-Karls-Universität Heidelberg, Institut für Umweltphysik, D-69120 Heidelberg, Germany.

K. Bächmann and S. Schlomski, Technische Hochschule Darmstadt, Petersenstrasse 18, D-64287 Darmstadt, Germany.

A. Hofzumahaus, F. Holland, L. Hoppe, S. Konrad, D. Mihelcic, P. Müsgen, H.-W. Pätz, H.-J. Schäfer, T. Schmitz, and A. Volz-Thomas, Institut für Chemie und Dynamik der Geosphäre, Forschungszentrum Jülich, D-52425 Jülich, Germany. (d.mihelcic@fz-juelich.de)

G. K. Moortgat, Max-Planck-Institut für Chemie, Division of Atmospheric Chemistry, Postfach 3060, D-55020 Mainz, Germany.

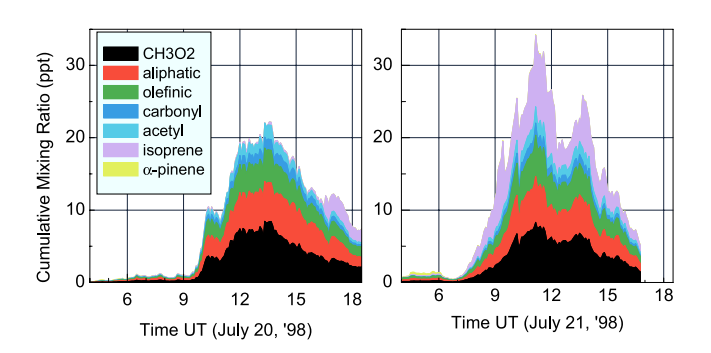
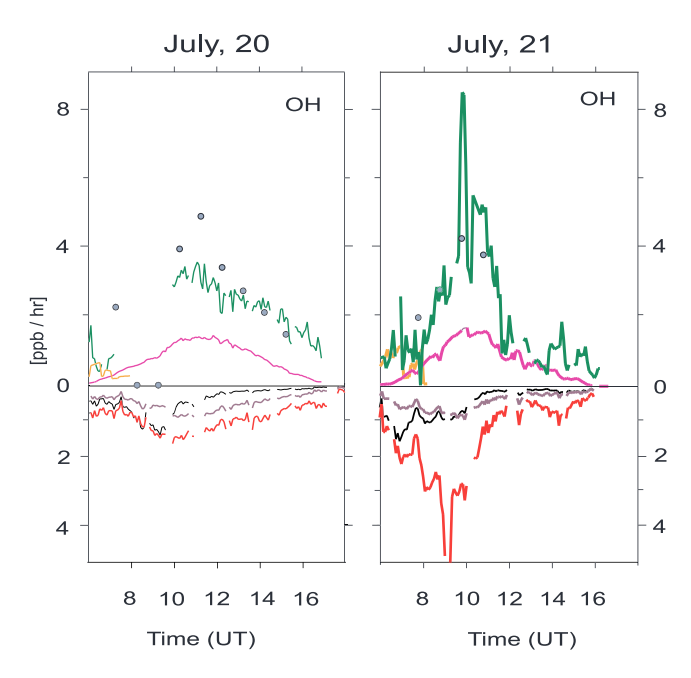
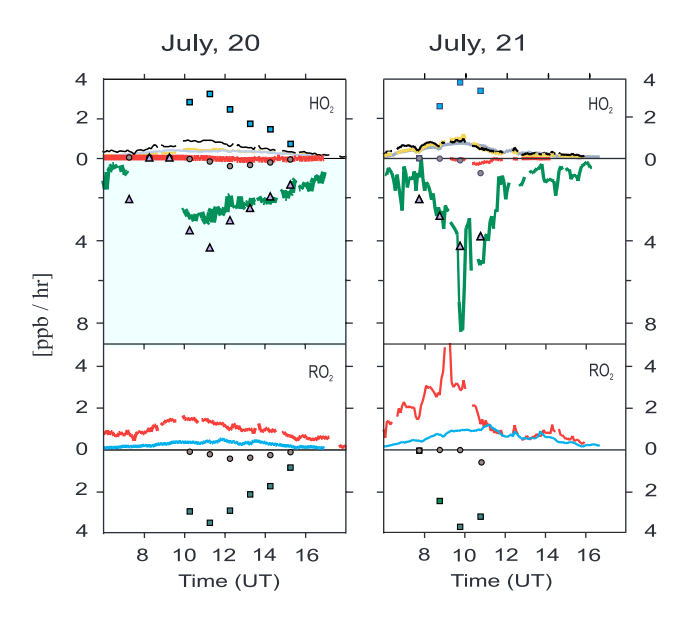


Figure 3. Speciation of RO<sub>2</sub> as calculated by the MCM for (left) 20 July and (right) 21 July.



**Figure 4a.** Major production and destruction rates of OH during (left) 20 July and (right) 21 July calculated from the observations. OH:  $k_2 \times HO_2 \times NO$  (green line: LIF, gray circles: MIESR);  $k_1 \times H_2O \times O(^1D)$  (pink line); J(HONO)  $\times$  HONO (yellow line); OH destruction:  $k_8 \times OH \times NO_2$  (black line);  $k_i \times OH \times VOC_i$  (red line);  $k_3 \times OH \times CO$  (brown line). All values are in units of ppb/hr.



**Figure 4b.** Major production and destruction rates of  $HO_2$  and  $RO_2$  during (left) 20 July and (right) 21 July calculated from the observations. (top)  $HO_2$ :  $k_5 \times RO_2 \times NO$  (blue squares);  $k_3 \times OH \times CO$  (black line);  $k_4 \times OH \times HCHO$  (yellow line);  $2J(HCHO)_{radical} \times HCHO$  (gray line);  $HO_2$  destruction:  $k_2 \times HO_2 \times NO$  (green line, LIF) and pink triangles (MIESR);  $k_{10} \times HO_2 \times RO_2$  (brown circles, MIESR);  $k_9 \times HO_2 \times HO_2$  (red line, LIF). (bottom)  $RO_2$ :  $k_i \times OH \times VOC_i + k_7 \times OH \times CH_4$  (red line);  $CH_3O_2$  production from PAN decomposition (blue line);  $RO_2$  Destruction:  $R_2 \times RO_2 \times RO_3$  (green squares);  $R_3 \times RO_3 \times RO_3 \times RO_3$  (brown circles, MIESR). All values are in units of ppb/hr.